LUND UNIVERSITY

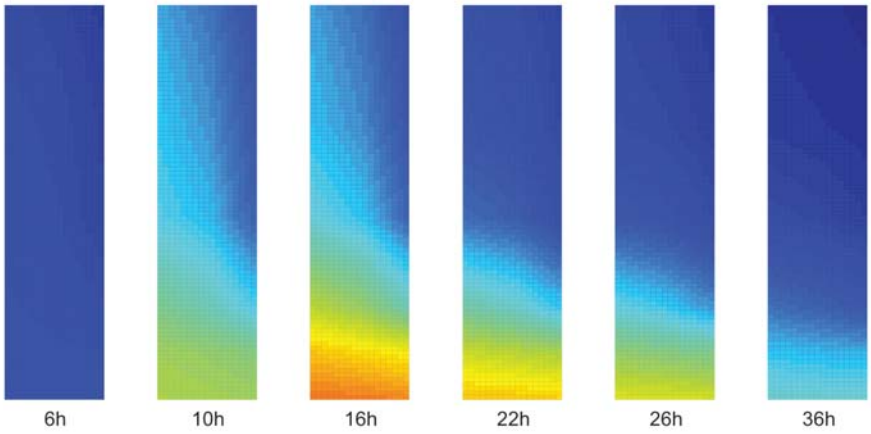

FINITE ELEMENT ANALYSIS OF TEMPERATURE IN HARDENING CONCRETE USING ISOTHERMAL CALORIMETRIC DATA

JOHN MAC

Structural Mechanics

Master's Dissertation

DEPARTMENT OF CONSTRUCTION SCIENCES

DIVISION OF STRUCTURAL MECHANICS

ISRN LUTVDG/TVSM--17/5221--SE (1-81) | ISSN 0281-6679

MASTER'S DISSERTATION

FINITE ELEMENT ANALYSIS OF TEMPERATURE IN HARDENING CONCRETE USING ISOTHERMAL CALORIMETRIC DATA

JOHN MAC

Supervisors: Professor **OLA DAHLBLOM**, Div. of Structural Mechanics, LTH, together with **JONAS LINDEMANN**, PhD, Div. of Structural Mechanics, LTH & Lunarc and Professor **LARS WADSÖ**, Div. of Building Materials, LTH.

Examiner: **SUSANNE HEYDEN**, Senior Lecturer, Div. of Structural Mechanics, LTH.

Printed by Media-Tryck LU, Lund, Sweden, June 2017 *(Pl)*.

For information, address:
Division of Structural Mechanics,
Faculty of Engineering LTH, Lund University, Box 118, SE-221 00 Lund, Sweden.
Homepage: www.byggmek.lth.se

Abstract

The produced heat in hardening concrete is of special importance to consider as the temperature rise within a large concrete structure can become such high that the structure may experience thermal cracking. With use of a simulation program that is based on the finite element method, the temperatures within the structure can be estimated to predict possible crack development.

The heat produced by the cement is normally modelled with conventional methods that is based on semi-adiabatic measurements. However, recently isothermal calorimetry has been discussed as a method that measures the heat of the cement more accurate.

The objective of this dissertation is to develop an algorithm to compute thermal power of hardening concrete using isothermal calorimetric data for finite element analysis. To examine how simulations with isothermal calorimetric data performs in comparison to the conventional method for thermal analysis of concrete, an experimental setup was built containing the same concrete as isothermal calorimetric data was attained for.

The implementation of the algorithm was successful and now HACON is able to perform simulations with isothermal calorimetric data. The conclusion of the thermal analysis is that simulation with the isoconversional method and with the conventional method gives slightly different results.

The experimental setup was also built successfully by Flemark [1], however, due to the complex air flow surrounding the setup, it wasn't possible to attain a definite conclusion whether finite element analysis based on heat calculations according to isoconversion is more accurate than the conventional method. The conclusion is that a program has been successfully developed but further work needs to be made to validate the accuracy.

Keywords: isoconversion, isothermal calorimetry, thermal analysis, finite element method, numerical simulation

Preface

This dissertation is submitted for the degree of Master of Science in Engineering, Civil Engineering at LTH, Lund University.

Firstly, I would like to thank my head supervisor Prof. Ola Dahlblom and co-supervisor Prof. Lars Wadsö for coming up with the initial idea for this dissertation and their excellent support and guidance, whose help have been invaluable throughout this process.

Furthermore, I would like to express my gratitude to my co-supervisor Ph.D Jonas Lindemann for the invaluable help with the programming, who have had an essential role of the implementation of the algorithm.

Finally, I take this opportunity to thank my friends and family for all their support throughout my years of education.

John Mac
Lund, June 2017

Contents

1 Introduction

1.1 Background

Mass concrete is a structural element with dimensions large enough to require actions to prevent excessive heat development. Such elements are mostly associated with structures such as dams, bridge piers and other structures with large volume placements.

Heat develops in concrete during hardening as a result of exothermic reactions between water and cement. If the produced heat is not dissipated to the environment, the temperature rise within a large concrete structure can become high and the structure may experience thermal cracking.

These issues are well known and there are several computer programs that are able to simulate the heat distribution in concrete. These simulation programs are based on finite element analysis (FEA), which is a numerical method used to predict real scenarios. Predicting heat profiles are one of many applications of FEA.

In order to perform good simulations, the heat that is produced by the reacting cement needs to be modelled accurately. There are standard methods that are used to measure the produced heat, which aim to resemble the generated heat of the cement. The result of these methods is a model of the heat production that is implemented in FEA programs.

Many of the standard methods have been around for many years, but recently isotherm calorimetry has been discussed as a method that measures the heat production more accurately than the standard methods.

Therefore, Prof. Ola Dahlblom and Prof. Lars Wadsö initiated the idea of implementing results from measurements using isothermal calorimetric data into a FEA program. Byberger [2] performed a study regarding the possibility to evaluate the temperature development in hardening concrete with the isoconversional theory which is based on isothermal calorimetry. This dissertation is a follow-up work and the aim is to implement an algorithm to calculate the temperature development in hardening concrete with isoconversional theory.

In this project the implementation will be made for HACON [3] and may result in one of the first programs to support isothermal calorimetric data. HACON was developed by Vattenfall Utveckling AB and the Division of Structural Mechanics at

LTH Lund University, in order to predict heat development in large castings.

This is a project in cooperation with Flemark [1], whom is submitting her dissertation for the Division of Building Materials and will take part in setting up the experimental setup in this project.

1.2 Aim and objective

Combining of HACON and isothermal calorimetry that is performed at the Division of Building Materials at LTH, Lund University, an improved simulation program to analyse heat development in concrete structures may be achieved. The aim is to demonstrate how data from isothermal calorimetry of cement can be used for any FEA program for concrete structures.

The primary objective is to define an algorithm and develop computer code for computing thermal power using isothermal calorimetric data. The developed code will be implemented to HACON. In a subsequent stage of the project, the temperature development in a cast concrete structure will be recorded and compared with results from simulation based on the conventional method and simulation based on the isoconversional method.

The secondary objective is to examine whether simulations with isothermal calorimetric data estimates temperatures more accurately than the conventional method. The casting of the concrete will be performed by Flemark [1] and the Division of Building Materials at LTH, Lund University.

1.3 Outline

- Chapter 1 introduces the background information of the problem, methods and the aim of this dissertation.
- Chapter 2 lays out general concepts of cement as material and the hydration process.
- Chapter 3 presents common calorimetry methods used in cement industry.
- Chapter 4 presents the algorithm used for the data and computation of the thermal power of cement.
- Chapter 5 presents the procedure when obtaining isothermal calorimetric data of the cement that was used in the experimental setup. Also analysis between the simulations with the conventional and isoconversional method is presented.
- Chapter 6 presents the concluding remarks and discussion of the analysis and experimental setup.

2 Cement

Isothermal calorimetry is a powerful tool that is widely used in the research area to understand cement hydration. To give a brief understanding of the underlying mechanisms of cement hydration with regards to the results obtained from the isothermal calorimetry, a few central concepts of cement hydration will be presented.

2.1 What is cement?

2.1.1 Mineral composition

Portland cement clinker is obtained through a pyroprocess by mixing precise proportions of limestone and clay with some additives. The pyroprocess operates at such high temperature, about 1450 °C, that the chemical reactions that transform the raw feed into clinker take place. Depending on the variations of the chemical compositions of the raw feed, adjustment of the proportions are made so that the four minerals that constitute the Portland cement clinker is attained. The principal minerals that constitute Portland cement clinker are [4]

- tricalcium silicate $SiO_2 \cdot 3CaO$
- dicalcium silicate $SiO_2 \cdot 2CaO$
- tricalcium aluminate $Al_2O_3 \cdot 3CaO$
- tetracalcium ferroaluminate $4CaO \cdot Al_2O_3 \cdot Fe_2O_3$

For convenience reason, the four minerals mentioned above are often given with pseudo-chemical notations from ceramic science, resulting in the following notations

- C_3S for $SiO_2 \cdot 3CaO$
- C_2S for $SiO_2 \cdot 2CaO$
- C_3A for $Al_2O_3 \cdot 3CaO$
- C_4AF for $4CaO \cdot Al_2O_3 \cdot Fe_2O_3$

2.1.2 Cement microstructure model

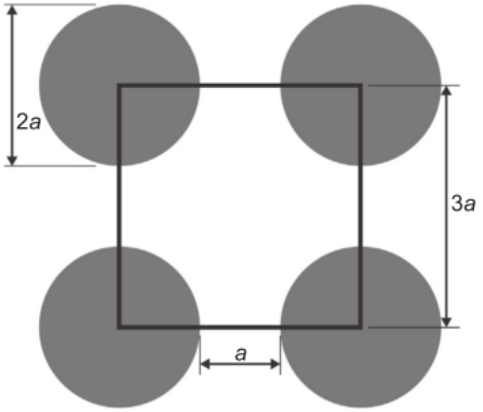

Figure 2.1: Idealised 2D model that represents a sliced image of a 3D cement structure

The water to cement ratio (w/c-ratio) is a central concept when describing the cement's microstructure. It has been demonstrated that the w/c-ratio actually is a number that is directly related to the average distance between the cement particles [5]. This is illustrated as a simplified two-dimensional model in Figure 2.1, which is a sliced image from a fictive 3D model of cement particles where the four circles are the cement particles. The radius of the circles is a and the circles are placed with the centre on the corners of a square with sides of $3a$. To study the microstructure of cement, only the square and the content inside is studied, as it can be recognised as the idealised homogeneous part of a cement, see Figure. 2.2. Between the particles, the intermediate part represents the water content.

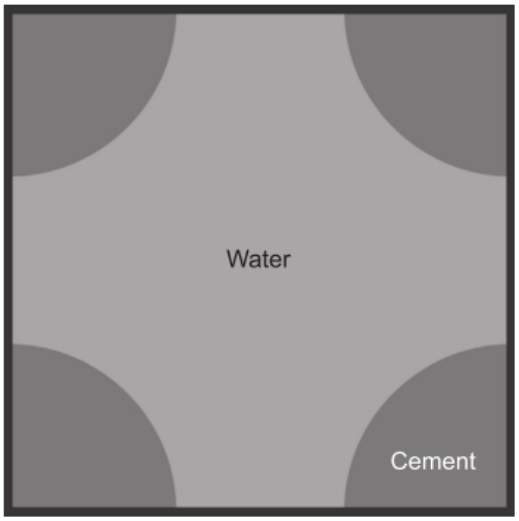

Figure 2.2: Idealised homogeneous part of the model in Figure. 2.1

In order to calculate the w/c-ratio for the model, the surface area of the square is first determined as $9a^2$ and secondly the particles' aggregated surface area is πa^2,

resulting that the mass of the water content becomes

$$w = 9a^2 - \pi a^2 = (9 - \pi)a^2. \tag{2.1}$$

Assume that the relative gravity for the cement is π, then the mass becomes

$$c = \pi a^2 \cdot \pi = \pi^2 a^2. \tag{2.2}$$

The w/c-ratio is then calculated as the mass quotient between the water and cement content, which gives

$$w/c = \frac{(9 - \pi)a^2}{\pi^2 a^2} \approx 0.6. \tag{2.3}$$

In comparison, a more compact structure with w/c-ratio of 0.14 is illustrated in Figure. 2.3. Although it's not a realistic w/c-ratio, the purpose is to illustrate how the w/c-ratio is related to the microstructure. The shortest distance in Figure. 2.2 is a, whereas in the denser structure the shortest length can be calculated to $0.12a$, see Figure. 2.3. Thus, by reducing the w/c-ratio the distance between the particles is also reduced.

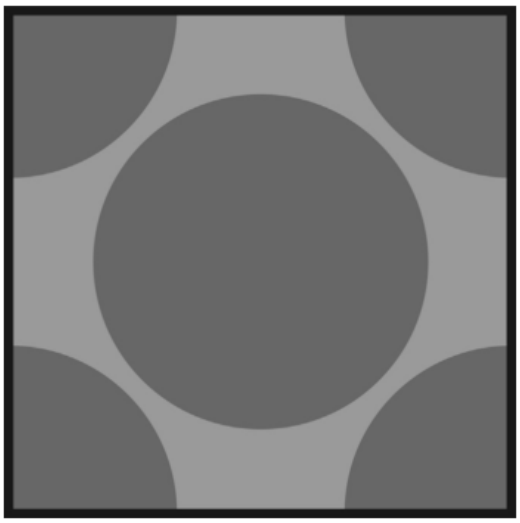

Figure 2.3: Denser 2D cement structure

The hydration products from the reaction have larger volume than the initial cement particles, resulting in that the water filled spaces between the particles is gradually replaced by the hydration products during the reaction. However, not all space is fully substituted and this creates what is traditionally defined as the capillary pore space. In the cement gel (presented in Section 2.1.4) there exists a significant volume of very small pores, gel pores. Thus, the pore system in the cement consists of the capillary pores and the gel pores [6].

The time it takes for the gel to make contact can be measured directly as the setting time of the cement. This means that during this period the casting of concrete can

be made as it is still workable. After this time, the workability decreases due to hardening of the cement.

It should be noted that the time it takes for the gel to make contact with the adjacent gel, is affected by the w/c-ratio. In Figure 2.3, the shorter distance between the cement particles will lead to shorter setting time compared to the one in Figure 2.2 and faster development of a dense structure.

2.1.3 Hydration of cement

The initial hydration reaction of the cement particle is dominated by reaction between C_3S and water, where the C_3S dissolves rapidly [7]. The initial reaction can be described according to

$$C_3S + 3H_2O \longrightarrow CSH + CH. \tag{2.4}$$

However, the precise chemical composition of calcium silicate hydrate varies, so it is written in the vague formulation as CSH. In Figure 2.4, the hydration process is illustrated, where it can be observed that as the growth of gel (CSH) increases, the cement particle dissolves.

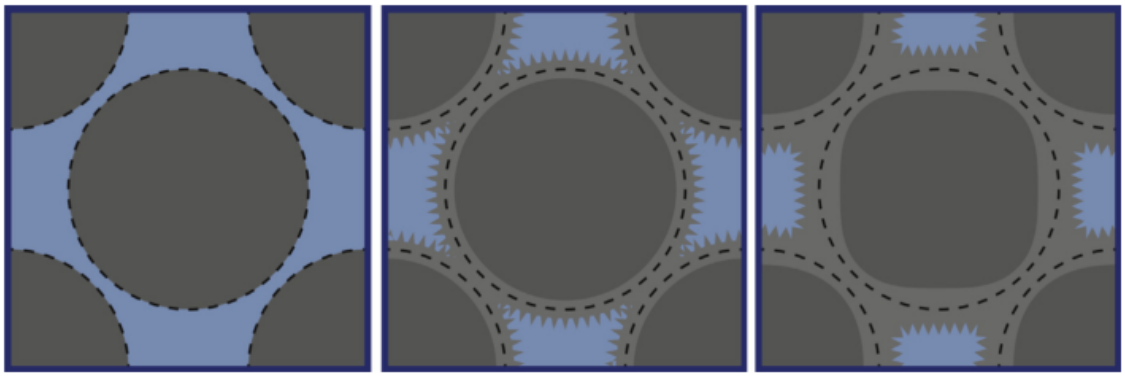

Figure 2.4: Cement hydration in three stages. In the left image the cement particles are still unreacted with the water. The image in the middle illustrates that after a short period, the cement particles have reacted with water and cement gel is created. In the right most image the cement gel has expanded further and more of the cement particles are dissolved.

The hydration products expand from the particles and fill the pores in the cement and it is the component of the cement that is responsible for concrete's final strength [8]. Besides the gel, a crystalline by-product, calcium hydroxide (CH), is also produced. Calcium hydroxide is also commonly named Portlandite [4]. Portlandite does not contribute to the strength of the hydrated cement in a Portland cement system, but in a blended cement the supplementary cement materials are transformed into secondary CSH by reaction with CH [9].

2.1.4 Morphology of cement gel

The morphology of the cement gel presents itself in two types. The first type is the outer product that develops on the surface of the cement particles and grows towards the pore space between the particles, resulting in fibrillar morphology. The second type is an inner product that fills the space of the originally anhydrous cement [8].

In previous work [7] nuclear resonance reaction analysis (NRRA) has been used to observe if there exists an inner and outer cement gel. In the research, it was observed that the hydrogen depth varies with depth and time, leading to the conclusion that there are different layers with varying porosity, where the outer product has notably larger porosity than the inner product. For more details the reader is referred to reference [7]. Figure 2.5 illustrates this idea, where the outer and inner layer of the cement gel has been contrasted.

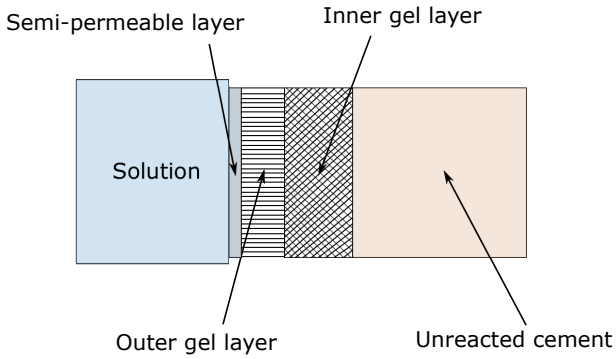

Figure 2.5: Cement gel inner- and outer product

2.1.5 Influence of hydration

The hydration influences early-age properties such as setting time, temperature rise and autogenous shrinkage, where the latter two are major contributors to early-age cracking of cement-based materials [10].

The reaction mechanism in cement is complicated as numerous reactions appear simultaneously, resulting in various rate of hydration for different cement types. The hydration process can be affected by several factors, mainly [11]:

- water-to-cement ratio (w/c-ratio)

The water-to-cement ratio is a parameter that controls the amount of water available for the hydration process and influences the final degree of hydration that can be achieved. Generally, concretes with higher w/c-ratio exhibits a higher degree of hydration than lower w/c-ratio [12]. According to Power's model of the cement hydration (described in section 2.1.2), the existing capillary pore space for concrete with w/c-ratio less than about 0.36, is insufficient to achieve complete hydration.

- fineness of cement

The hydration rate has a direct relation to the thermal power [W/kg], details in Section 3.3, which can be measured with a heat conduction calorimeter. The authors in reference [11] performed a study, by considering the fineness of the cement, where it was observed that the use of cement with higher fineness accelerates the hydration reaction due to the increase of surface area available to react with water [13, 11]. The effect of the fineness decreases with the degree of hydration, where in early periods of the hydration process, the fineness has larger influence than at later stages due to the denser structure which restricts the reaction between water and cement [14]. Comparing the results from Figure. 2.6 and 2.7, the results show that the rate of heat of hydration is higher in early stages for cement A, containing cement of higher fineness, than cement B that was composed with coarser components.

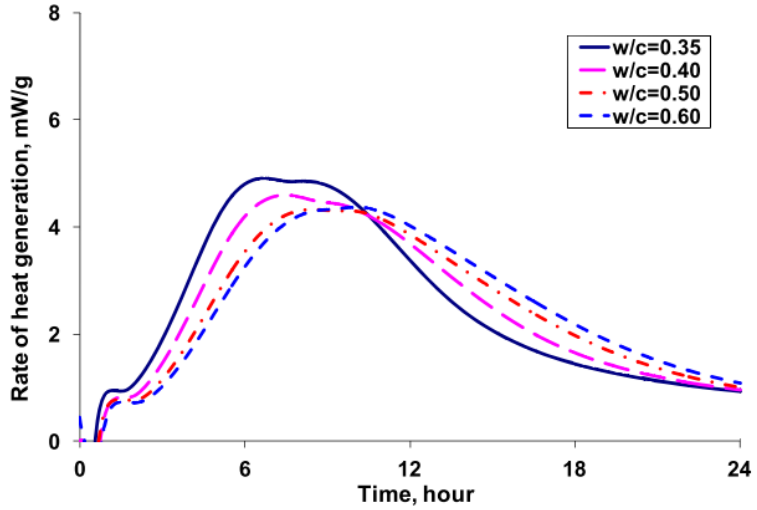

Figure 2.6: Cement A, rate of heat of hydration for fine cement

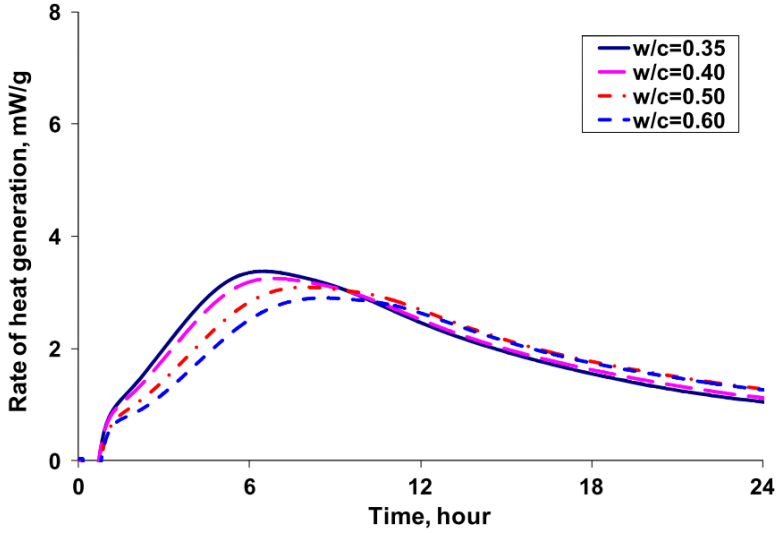

Figure 2.7: Cement B, rate of heat of hydration for coarse cement

- chemical properties of the cement

The chemical composition affects the hydration in various ways. Depending on the composition of C_2S and C_3S, the resulting CSH varies and proceeds with different heat developments. The effect from added CSH has been studied in previous work where it was concluded that the amount of CSH influenced the induction period and the following peak. The added CSH resulted in more CSH precipitating at early period and consequently leading to an increase of the maximum heat rate as seen in Figure 2.8 [8].

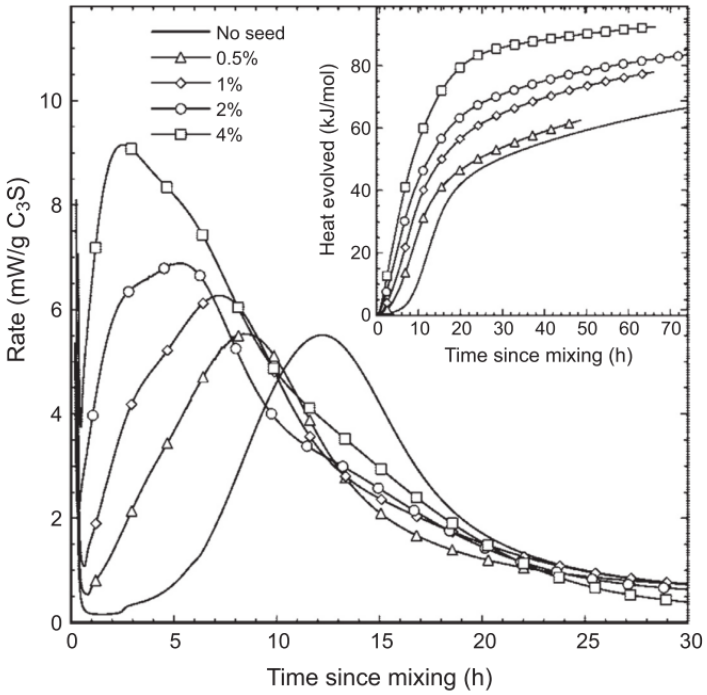

Figure 2.8: Impact on hydration kinetics of C_3S by addition dosages (percentage by weight of C_3S) of CSH seeds. Reproduced from [8]

2.2 Hydration periods

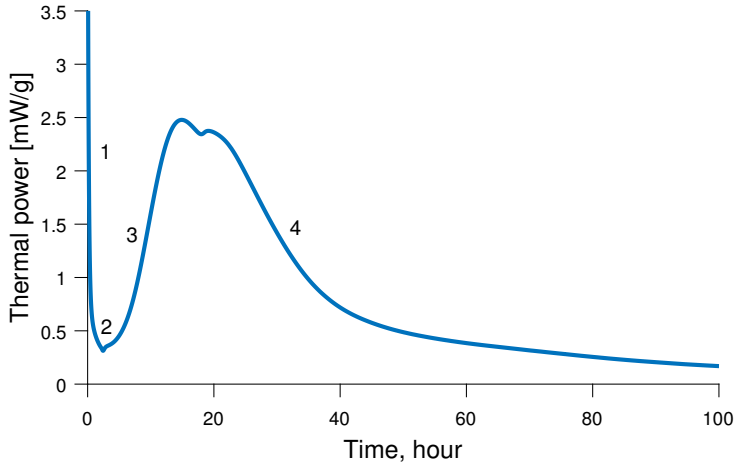

Figure 2.9: Schematic power output from cement hydration. The numerical figures denotes each period of cement hydration.

Results from isothermal calorimetry measurements indicate distinct periods of cement hydration, where each period is not yet fully understood and studies in the research area are progressed to explain the phenomena that arise. This section presents some hypothesis of each period that is currently prevailing. In Figure 2.9 results from an isothermal measurement can be observed, where the different periods of cement hydration are identified with a number, which are recognised as

1. Initial period
2. Induction period
3. Acceleration period
4. Deceleration period

2.2.1 Initial period

The initial period starts by the wetting of cement and is characterised by the peak that is noticeable in period 1, that is a result by the dissolution of C_3A which leads to a highly exothermic reaction that only lasts for a short time. In the initial period the proceeding reaction of the initial peak is a rapid deceleration that is not yet fully understood. This period is difficult to study because of the high rates of the processes and the difficulty to stop the hydration without creating artefacts [15]. Various controversial hypotheses have been proposed in the research area to explain the initial decrease. Below, one explanation of the decrease is presented, that is one amongst many other which has wide plausibility [7].

One hypothesis considers a metastable membrane of CSH that forms around the anhydrated cement and it is suggested that it's only permeable for some ions, which

causes the deceleration of hydration. As the membrane is formed, the surface is passivated since only calcium, not silica, is able to pass through the membrane to the solution (pore water) that leads to an increase in concentration of silica inside the membrane. The effect is that the high concentration of silica inside the membrane sets up an osmotic pressure and as the pressure becomes high enough, the water is transported into the silica-concentrated segment and eventually causes the membrane to break. This results in rapid conversion of the intermediate silicate hydrate phase into CSH, resulting in the acceleration observed in period 2 [8, 7, 16]. For further details and an overview of other hypothesis the reader is referred to reference [7].

2.2.2 Induction period

The induction period is characterised as the period where low heat evolution occurs between period 1 and period 3. This period is considered as a separate period by some authors, but according to the author in reference [7] this is only a consequence of a reduced reaction rate of the previous period until the critical point is reached. That is when the rate of nucleation and growth of CSH starts to accelerate. Until the beginning of the acceleration period the total degree of hydration is typically 0.1 to 1 percent [17].

2.2.3 Acceleration period

The authors of reference [18] proposed that the increased nucleation and growth of a stable form of CSH causes the acceleration in period 3. Basically, the hypothesis covers conversion of a metastable CSH to a stable form of CSH, that gives rise to the acceleration observed in period 3. Experiments described in reference [19] observed these types of cement gel morphology and verifies the idea of a metastable and a stable CSH. Once the stable CSH has been nucleated, either within the surface of C_3S or in close proximity, growth of the new phase can occur by precipitating hydrates into the pore space. This implies that it is the growth of the stable hydrates that controls the rate of dissolution of C_3S [17].

The importance of the presence of stable CSH nuclei for further growth has been shown in the study of reference [20], where artificially prepared stable CSH seeds were added with the cement and water solution. The result indicated that the hydration of C_3S accelerated notably and affected the onset of the acceleration period to begin earlier and increasing the rate of the main peak [17]. The results from the experiment are presented in Figure 2.8.

The authors of reference [8] concluded that this implies that the induction and the acceleration periods are controlled by the nucleation and growth of stable CSH, which is coupled with C_3S dissolution. If growth of CSH controls the rate of the main peak, then the rate of hydration is proportional to the surface area of CSH [7].

2.2.4 Deceleration period

In comparison to the quantitative studies of the earlier periods of the hydration (period 1 - 3), the studies in the later periods are fewer [7]. Several factors that could contribute to the slower hydration rates in period 4 are many, most obvious factors could be:

- lack of space
- lack of water

The lack of space is motivated as it has been experimentally observed by the authors in reference [21] that quantified varying growth rates parallel and perpendicular to the cement particle with use of atomic force microscopy (AFM). The hypothesis that reference [8] concludes from the results on the experiment is, until full coverage on the surface is reached, the precipitated CSH will proceed in parallel and perpendicular direction to the surface of C_3S. As full coverage is obtained, the decrease in rate of hydration is explained by a procedure of hydration only in perpendicular direction on the previously formed CSH. As the rates continue to decrease in period 4, the explanation is that the process becomes diffusion controlled because of the transition to a denser hydrate regime in the microstructure, contributing to a limited transport of water for the growth of CSH.

Lack of water is particularly important. Since the total volume of hydrates is slightly lower than the combined volume of the cement and water, known as chemical shrinkage, leads to formation of gas-filled pores in the structure. This results in a decrease of the internal relative humidity and decreases the hydration rate [8].

2.3 Maturity concept

The maturity of concrete is a concept that combines the effects of time and temperature as a result from hardening concrete, which can be used as an indication of the concrete's age at a time t [22]. The maturity concept has gained widespread acceptance in the concrete industry and has been further developed by Hansen and Pedersen, who proposed to base the maturity concept on the Arrhenius equation [23]. With use of the Arrhenius equation, the nonlinear maturity of the concrete is being taken into account and is considered to be more accurate as it better represents the effect of temperature on development of mechanical properties of concrete at early age [24].

The maturity is expressed as the equivalent age, which is the actual curing age t [hour] of a concrete cured at any temperatures T [Kelvin] converted to an equivalent curing age t_e [hour] for a specimen cured at a specific reference temperature T_{ref}, normally 293 Kelvin (20 °C). The equivalent age t_{e} of the concrete is obtained as

$$t_{\mathrm{e}} = \int_0^t e^{\theta\left(\frac{1}{T}-\frac{1}{T_{\mathrm{ref}}}\right)} \mathrm{d}t \tag{2.5}$$

and θ is an empirical parameter, expressed as

$$\theta = \theta_0 \left(\frac{T_{ref} - T_a}{T - T_a} \right)^{\kappa_0} \tag{2.6}$$

where

θ_0 and κ_0 are material parameters

T_a is a constant chosen as $T_a = 263$K (-10°C)

t_e [hour] is the equivalent age at reference temperature T_{ref}

T [Kelvin] is the curing temperature that can vary in time and

t [hour] is the specimen's actual age.

2.4 Degree of hydration

The degree of hydration of cement is a central concept which indicates how far the cement has hydrated. It is an important parameter when working with cement, as it is used in order to evaluate the properties of cement, such as setting time, compressive strength etc. Therefore, experimental and mathematical methods to evaluate the degree of hydration is introduced.

2.4.1 Estimating the degree of hydration

The degree of hydration is a measure of the cement that defines the fraction of cement that has hydrated with water at time t. The degree of hydration α has the interval (0,1) where $\alpha = 0$ implies that no reaction between the cement and water has occurred [14], practically meaning that the concrete components is not blended together, considering that reaction starts as soon as cement makes contact with water. For $\alpha = 1$ theoretically all cement has hydrated, however, in practice full hydration is never achieved as the dense microstructure restricts the water from the cement particles. However, it should be noted that the hydration variable α does not describe the true hydration process in any detail but is a useful measure of how far the hydration has gone [14]. Figure 2.10 is an illustration of the development of the degree of hydration.

As the hydration is a complex process it is difficult to find one function that expresses the amount of cement which has hydrated. Several ways are proposed to express the degree of hydration, either calculating the degree of hydration with measurements of chemically bound water as

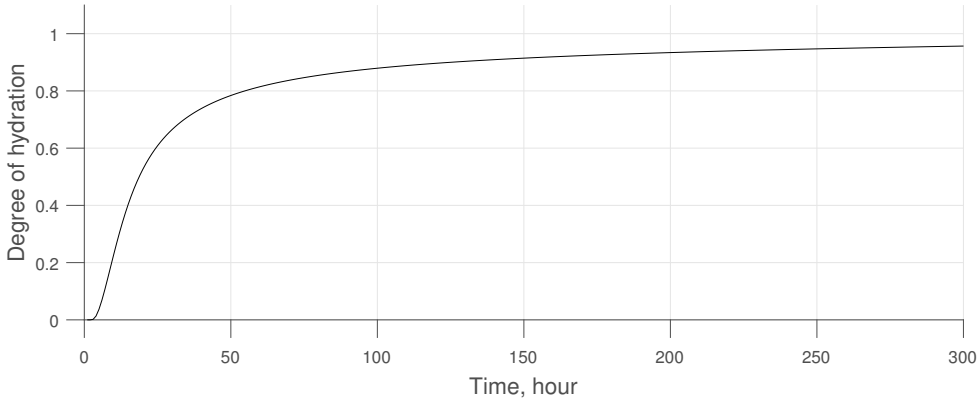

Figure 2.10: Schematic development of the degree of hydration

$$\alpha = \frac{w}{w_\infty} \tag{2.7}$$

where

$w = w(t)$ is chemically bound water at time t, kg/m^3

$w_\infty = w(t_\infty)$ is chemically bound water at complete hydration kg/m^3

or generated heat as

$$\alpha = \frac{Q}{Q_\infty} \tag{2.8}$$

where

$Q = Q(t)$ is generated heat of hydration at time t J/kg

$Q_\infty = Q(t_\infty)$ is generated heat of hydration at complete hydration $\alpha = 1$, J/kg.

The two ways give similar results, although, one or the other can be more or less practical depending on the study that is performed. The generated heat is quite easily measured and is a common approach used in the cement industry. There are several methods that can be used in order to measure the heat output which are addressed in Chapter 3

2.4.2 Heat of hydration

As heat develops from the chemical reaction it's of interest to model the heat development to predict and take into account various succeeding effects accompanying the hydration process. The heat can be measured in several ways, most commonly are adiabatic, semi-adiabatic or isothermal calorimetry, described in Chapter 3. In Figure 2.11 a schematic heat development for cement is illustrated.

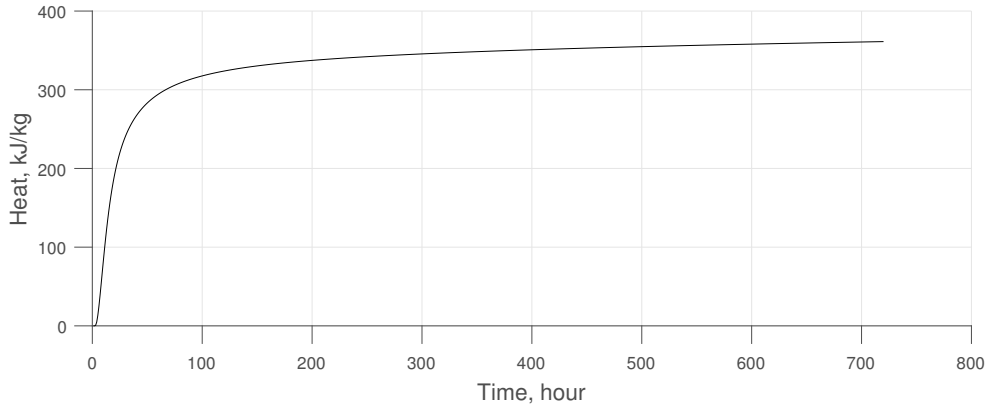

Figure 2.11: Schematic heat development of cement

With knowledge of the final heat Q_∞ that is produced from the hydration of a certain type of cement, the heat Q_n produced at time t can with use of Eq. 2.8 be expressed as.

$$Q = Q_\infty \alpha \tag{2.9}$$

Note that the heat is assumed to be proportional to the degree of hydration α.

The conventional method that most simulation programs use bases the calculation of the heat on the method presented in [25], which is a method based on data from semi-adiabatic measurements, described in Section 3.2. With use of isothermal measurements, the improvements in the accuracy of the heat will possibly be considerable. This is true because in the measurement with heat conduction calorimetry, the actual generated heat is measured, which leads to significantly less corrections of the measurements than with semi-adiabatic methods.

2.4.3 The conventional method - Degree of hydration as a mathematical function

In Eq. (2.9) the hydration α is apparent, but the parameter is defined differently depending on the situation where it is used. For experimental testing the equations expressed in the previous section are useful, however, in simulation and for the purpose of estimating a heat development at a time t a mathematical function is used. The author in reference [26] proposed that the degree of hydration in Eq. (2.9) could be expressed as

$$\alpha = e^{-\lambda_1 \ln\left(1+\frac{t_e}{t_1}\right)^{-\kappa_1}} \tag{2.10}$$

For various cement types, measurements have been made where the fitting parameters λ_1, t_1 and κ_1 are defined in programs, such as "Produktionsplanering Betong"

[27]. The fitting parameters are only regarded as mathematical tools that can be determined from heat curves. For different cement types, the hydration procedure are different and the fitting parameters is therefore unique for each cement. In Figure 2.12 various fitting parameters have been tested, resulting in various hydration rates, most notable in early period. In Table 2.1 the parameters used in Figure 2.12 are presented.

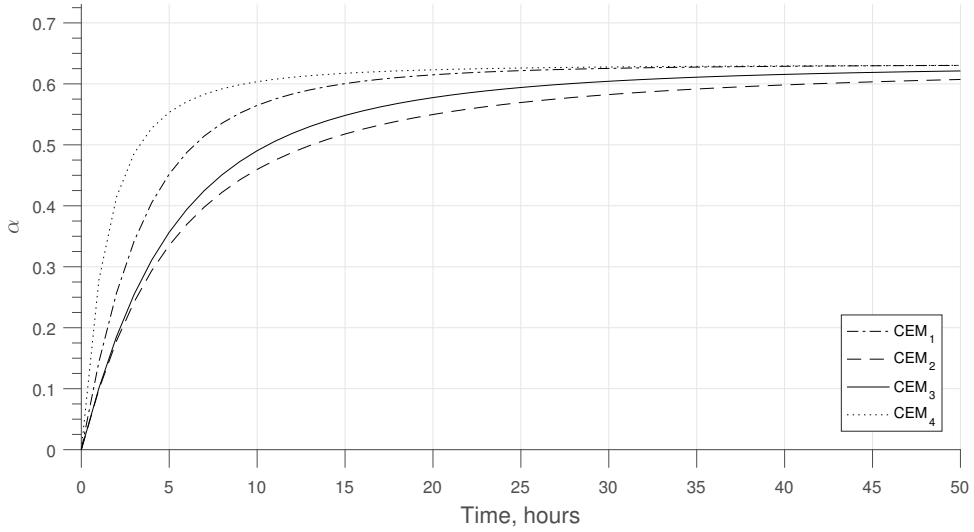

Figure 2.12: Hydration developments for fictitious cements in table 2.1

Table 2.1: Parameter values of Eq. (2.10) for cement types in Figure 2.12

	λ_1	t_1	κ_1
CEM_1	1.000	7.000	3.000
CEM_2	1.000	5.294	1.569
CEM_3	1.000	7.487	2.214
CEM_4	1.000	1.818	1.892

3 Calorimetry

Calorimetry is an experimental technique that is performed with a calorimeter. It is regularly used in science to measure heat associated with different energetic effects from physical and chemical processes of the examined sample. Most FEA programs bases the numerical routines on heat curves, that are obtained by adiabatic or semi-adiabatic calorimetry, recognised as the conventional method in this dissertation. The reader will be given a description of these calorimetric methods. Finally, the theory of isothermal measurements will be presented.

3.1 Adiabatic

3.1.1 Adiabatic instrument

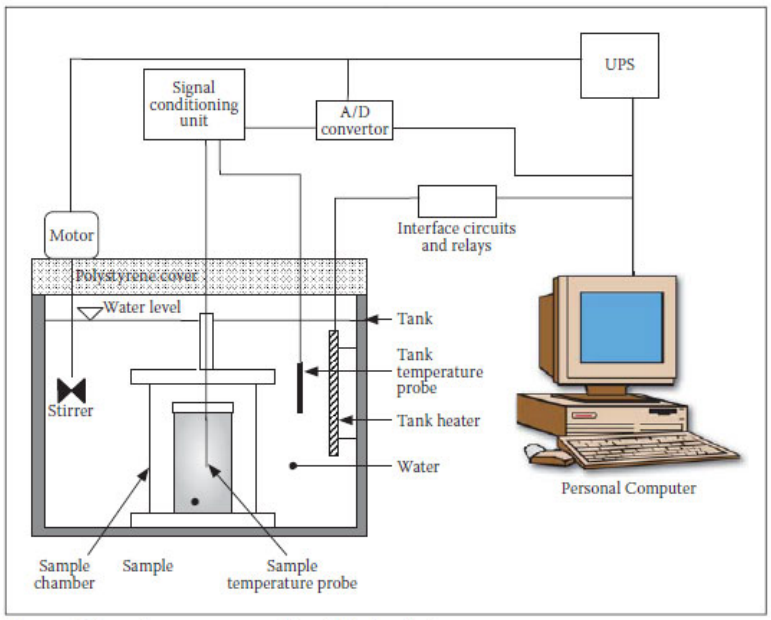

Figure 3.1: Illustration of an adiabatic setup

Adiabatic methods aim to eliminate the heat exchange between the sample (concrete) and the setup during the reaction, which in an ideal case implies that the setup itself doesn't have any impact of the result. Most modern adiabatic devices

accomplish to minimise heat loss from the test cell by maintaining the temperature of the setup equal to the temperature of the sample, resulting in no heat exchange [28].

The adiabatic calorimeter for concrete, which is schematically shown in Figure 3.1, operates so that the adiabatic condition is maintained by regulating the water in the tank. The sample is placed in the calorimeter and as the sample's temperature increases, the heater turns on or off to keep the water temperature apace with the temperature of the sample.

3.1.2 Adiabatic calorimetry

In thermodynamics, the adiabatic process is defined such that no heat transfer occurs between the thermodynamic system and its surroundings. To model the heat development of cement, the adiabatic temperature curve is therefore measured and subsequently the temperature is recalculated to heat developed by the cement [28].

The advantage of the adiabatic calorimetry is that the measured temperature of the sample in an adiabatic calorimeter is at any time very close to the true adiabatic temperature. Therefore, influence of the change in reactivity of the cement is directly considered [28]. With the semi-adiabatic method the reactivity is taken into account by mathematical corrections and may involve uncertainties of the reactivity of the cement.

In Figure 3.2, it is illustrated how the temperature development for a true adiabatic situation could proceed. It should be noted that the temperature can reach over 50°C in large placements.

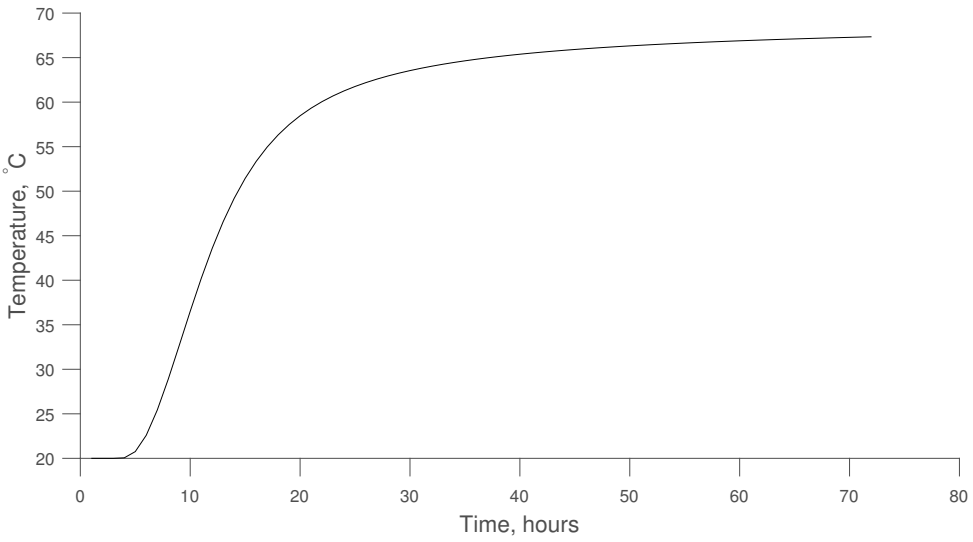

Figure 3.2: Schematic representation of adiabatic temperature rise of concrete

3.2 Semi-adiabatic

3.2.1 Semi-adiabatic instrument

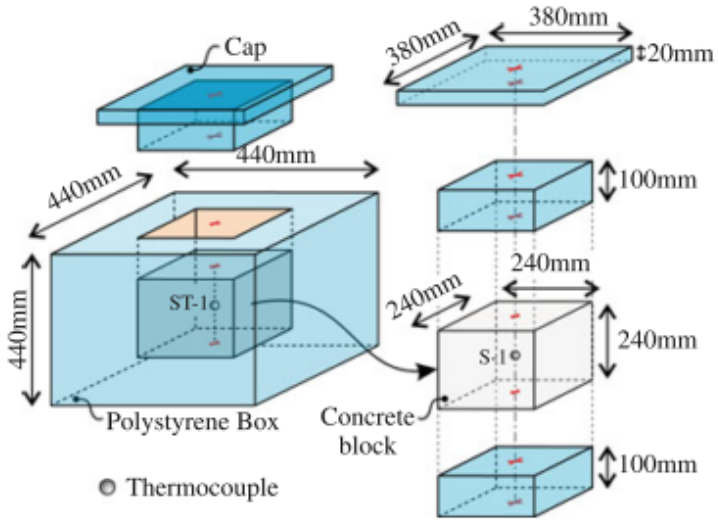

Figure 3.3: Illustration of a semi-adiabatic setup

As opposed to the adiabatic calorimeter, the semi-adiabatic measurement is performed such that the sample's heat is allowed to slowly dissipate from the setup. When the measurements of the temperature in the setup is obtained, the produced heat within the sample is possible to calculate with knowledge of the heat capacity, activation energy and the heat loss. These parameters are accounted for the evaluation process either with heat flow sensors installed in the insulation or calculated with heat loss coefficients [29].

There are different standard setups that are used, but the principal setup consists of a block of insulation material with room for a concrete block to be placed in. Most commonly some type of cellular plastic is used due to its homogeneous properties. The semi-adiabatic setup is extensively used because of its simplicity and availability, however, to make use of the result, it must be noted that it is likely that errors could occur if the setup isn't made well. In the work of reference [30] and [28] it's concluded that it is of high importance to consider the heat stored in the setup and it should be accurately known to receive accurate results.

3.2.2 Semi-adiabatic calorimetry

The authors in reference [30] proposed a semi-adiabatic setup that would increase the accuracy from the measurements, but still concluded that even with the developed setup, the temperature was still underestimated. As a result of the underestimated

temperature rise, the risk of cracks is obvious or the safety factor is significantly reduced.

The conclusion from reference [30] confirms what have been discovered in earlier research, where the author in reference [28] illustrates typical results from an adiabatic and semi-adiabatic measurement, see Figure. 3.4. The temperature measured with the adiabatic method is usually only slightly lower than the adjusted temperature curve, whereas for the semi adiabatic, the result considerably differs with much lower temperatures than the adiabatic temperature. The explanation from [28] is that the lowering of the temperatures in the semi adiabatic setup, will also influence the reactivity and consequently the correction applied for the measured temperature will still lead to a temperature rise which is still an underestimation of the adiabatic temperature.

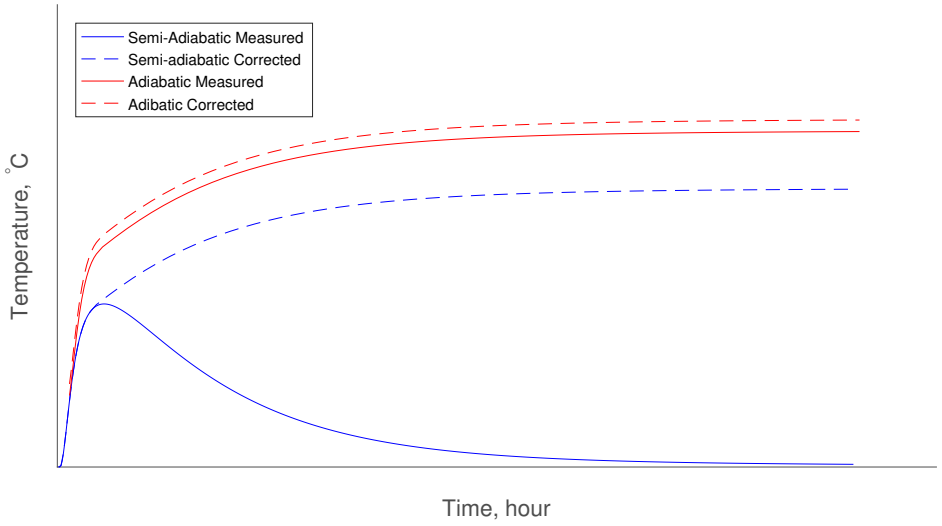

Figure 3.4: Comparison between semi adiabatic and adiabatic measurements before and after corrections

Even though the semi-adiabatic isn't the best method to model the heat development, it is still considered good enough for thermal simulation [31]. Another factor that makes the method much used is, as stated earlier, its simplicity and availability.

3.3 Isothermal

Isothermal measurements have wide applicability in the research of cement hydration. Typical applications are to study the response of the hydration of the cement when certain admixtures are used.

Simon [32] claims that for non-isothermal kinetics, as in cement kinetics where the curing results in temperature rise, traditional methods give highly uncertain values

of Arrhenius parameters and proposes that a model-free approach should be used, based on the isoconversional method.

3.3.1 Isothermal calorimetric instruments

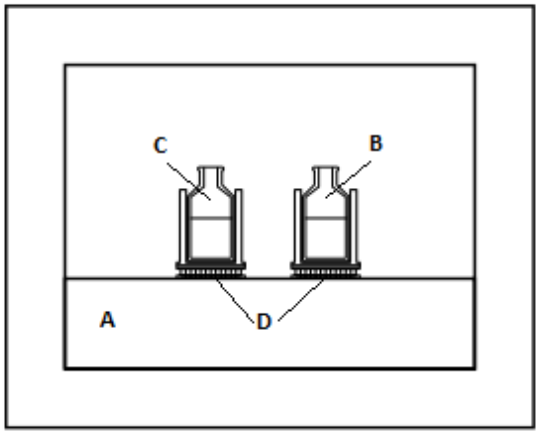

Figure 3.5: Schematic image of a twin design in a heat conduction calorimeter. A: Heatsink, B: Sample, C: Reference, D: Thermocouples plates

The heat-conduction calorimeter is made of a twin-channel design, consisting of a sample and a reference vessel that is connected to a heatsink through a heat-flow sensor. The heatsink is also connected to a thermostat that holds a constant temperature. Any deviations in temperature of the heatsink will restore its temperature to the one that is set in the thermostat. The unit is placed in an thermostated insulated container to protect it from the environment.

The heat-flow sensors used in most commercial heat-conduction calorimeters are thermocouple plates, TCPs, that produce a voltage induced by thermoelectric effects. For small temperature differences, it can be assumed that the voltage is proportional to the temperature difference. As the heat flow is proportional to the temperature difference, the voltage will also be proportional to the heat flow [33]. The techniques used in isothermal conduction calorimetry, and in other calorimetric instruments with twin design, doesn't measure the produced voltage between the sample and the heatsink. It's rather the difference between the sample and the reference that is recorded, simply by calculating the difference between the signal from the sample to the heatsink and the signal from the reference to the heat sink [33]. As a result of recording the difference of the signals, a significantly reduced noise is achieved [33].

The configuration of the heat conduction calorimeter is illustrated by the simple thermal model in Figure 3.6. The sample in the model is recognised by "A", where heat is produced as a result of chemical reactions, leading to heat dissipation from the sample into the heatsink, illustrated by "H". The produced heat increases the

temperature in the sample and the heatsink. If the setup is made properly, the increase of the heatsink will be much less noticeable as the heat capacity is much larger than for the sample. The heat flow will be conducted away to thermostat "O" but also backwards to the reference "B", resulting in a small temperature increase when heat is produced in "A". Thus, the importance of choosing a proper reference material is reflected here as the heat will affect the reference material.

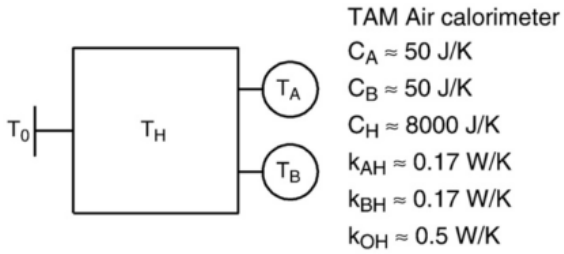

Figure 3.6: Schematic model of heat conduction calorimeter

It is essential that the reference and the sample is balanced in regard to the heat capacity. Although it's practically impossible to configure the reference to be exactly identical with the sample, one should balance the heat capacity within a 5% range of the sample [33]. Likewise, the reference sample should always be inert over the temperature range that is studied to avoid any disturbances of the measurements.

3.3.2 Isoconversion theory

The isoconversional methods are often used to describe the kinetics of solid-state processes [32] and has become more of use the last decade in cement research due to its advantage of describing very complex processes. It becomes handy as the cement chemistry consists of many different states in the process, going from liquid to solid-state. The fundamental principle with the isoconversional method is that the assumption of the rate of the conversion $d\alpha/dt$ is a function of two parameters: temperature T and conversion α [32],

$$\frac{\mathrm{d}\alpha}{\mathrm{d}t} = \Phi(T, \alpha) \tag{3.1}$$

Further, the function $\Phi(T, \alpha)$ is assumed to be expressed as the product of two functions independent of each other [32], where the first function $k(T)$ depends only on the temperature and the second depends only on the conversion $f(\alpha)$. The rate of the process can then be described as

$$\frac{\mathrm{d}\alpha}{\mathrm{d}t} = k(T)f(\alpha) \tag{3.2}$$

The function $k(T)$ is usually considered as the temperature-dependent rate constant and $f(\alpha)$ is considered as the conversion function that reflects the mechanism of the solid-state process [32].

In cement research, it is assumed that the temperature dependence follows the Arrhenius equation, resulting in that the rate constant can be expressed as

$$k(T) = Ae^{-\frac{E}{RT}} \tag{3.3}$$

where

A is the pre-exponential factor

E is the activation energy

R is the gas constant

T is the temperature

With Eq. 3.2 it becomes possible to observe the rate of hydration in relation to conversion rather than time, which offers a new approach to solve hydration kinetics.

At a constant extent of conversion α, the reaction rate is only a function of temperature. Taking the logarithm of Eq. (3.2) gives

$$\ln\left(\frac{d\alpha}{dt}\right) = \ln k(T) + \ln f(\alpha) \tag{3.4}$$

and taking the derivative of Eq. 3.4 with respect to T^{-1} yields

$$\left[\frac{\partial \ln(\mathrm{d}\alpha/\mathrm{d}t)}{\partial T^{-1}}\right] = \left[\frac{\partial \ln k(T)}{\partial T^{-1}}\right] + \left[\frac{\partial \ln f(\alpha)}{\partial T^{-1}}\right] \tag{3.5}$$

For constant α, it also implies that $f(\alpha)$ is constant, resulting that the second term on right-hand side of Eq. (3.5) becomes zero and with use of Eq. (3.3), the expression

$$\left[\frac{\partial \ln(\mathrm{d}\alpha/\mathrm{d}t)}{\partial T^{-1}}\right] = -\frac{E}{R} \tag{3.6}$$

is obtained. From Eq. (3.6) the advantages of isoconversional method can be observed. It can be noted that the temperature dependence of the process can be used to evaluate the value of the activation energy E, without determining any particular form of reaction model. That is the reason the isoconversion method is referred to as a model-free technique [34].

3.3.3 Isothermal calorimetry

This section regards the application of the isoconversion theory to isothermal measurements. In Figure 3.7 is an example of results from several isothermal runs of a process that proceeds according to a first order reaction. The output is the thermal power P in relation to time.

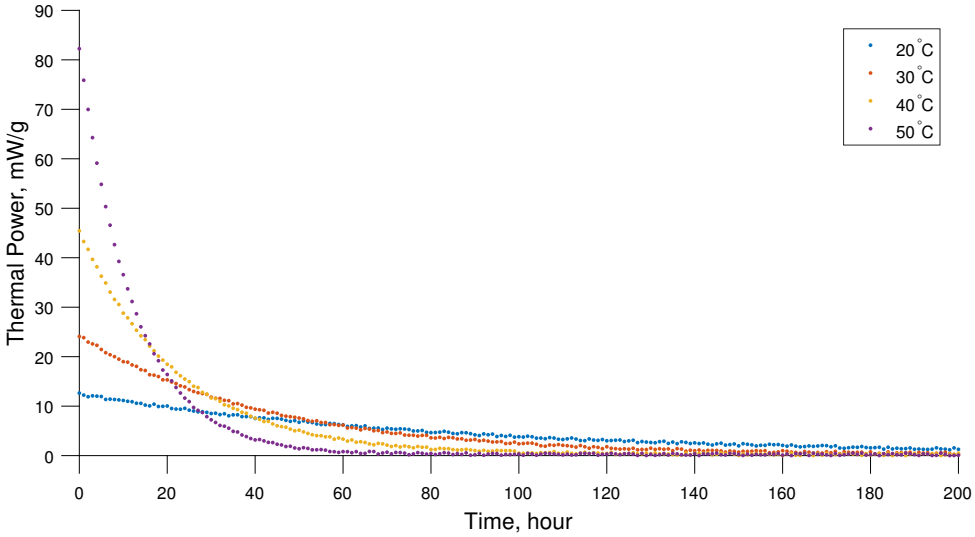

Figure 3.7: Thermal power $P(t)$ of a first order conversion with added noise for several isotherms

By integrating the thermal power P, the heat is obtained as

$$Q(t) = \int_0^t P(\tau)\mathrm{d}\tau \tag{3.7}$$

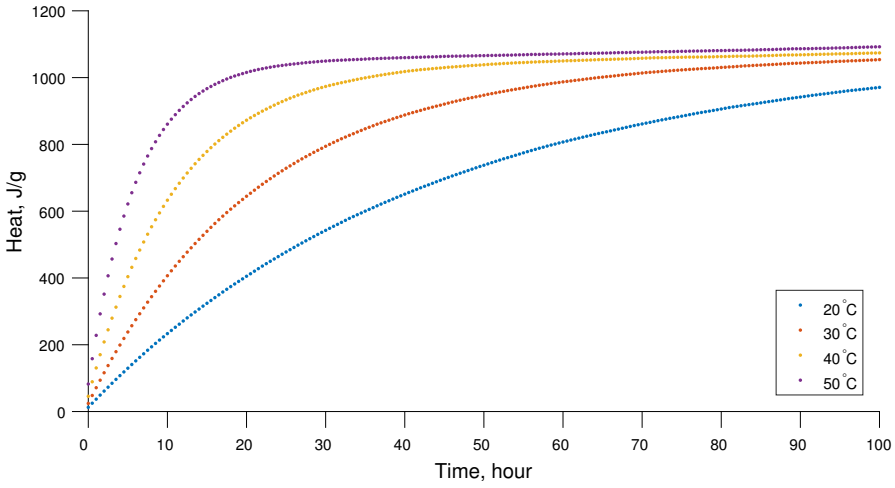

Figure 3.8: Heat $Q(t)$ of a first order conversion for several isotherms

According to the author in reference [29], it is possible to establish data for the thermal power P [W] for constant temperatures that is related to the rate of the process by the enthalpy Δh [J/g]

$$\frac{P}{\Delta h} = \Phi(T, \alpha) = k(T)f(\alpha) \tag{3.8}$$

With use of Eq. (2.8), the expression in Eq. (3.8) can be expressed as

$$\frac{P}{\Delta h} = \Phi\left(T, \frac{Q}{Q_\infty}\right) \tag{3.9}$$

Furthermore, it should be noticed that the enthalpy and the ultimate heat Q_∞ is not often known and according to the author in reference [29], it is possible to incorporate these parameters as

$$P = P(T, Q) = k(T)f(Q) \tag{3.10}$$

With use of the output obtained in Figure. 3.7 and Figure. 3.8, Eq. (3.10) is achieved by plotting the thermal power in relation to heat as shown in Figure. 3.9.

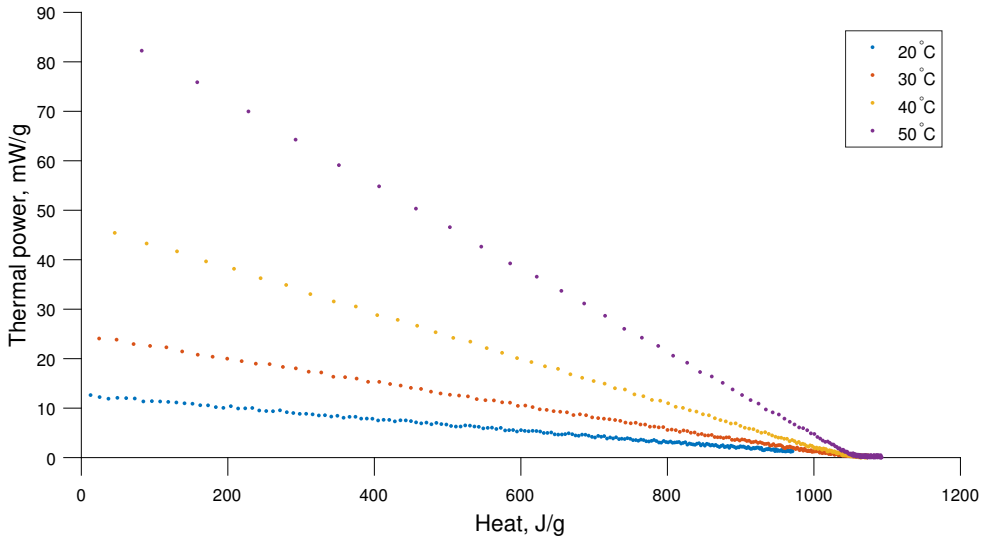

Figure 3.9: Isoconversion obtained by plotting thermal power against heat. Thermal power $P = P(T, Q)$

At a constant heat Q, the rate of the process which is measured as the thermal power, becomes a function dependent on the rate constant $k(T)$. Thus, Eq. (3.10) takes the expression [29]

$$P = P(T) = Ae^{-\frac{E}{RT}} \tag{3.11}$$

In Figure 3.10 the thermal power is extracted for each isothermal run. The extracted thermal powers are then plotted in the domain $P(1/T)$ as seen in Figure 3.11.

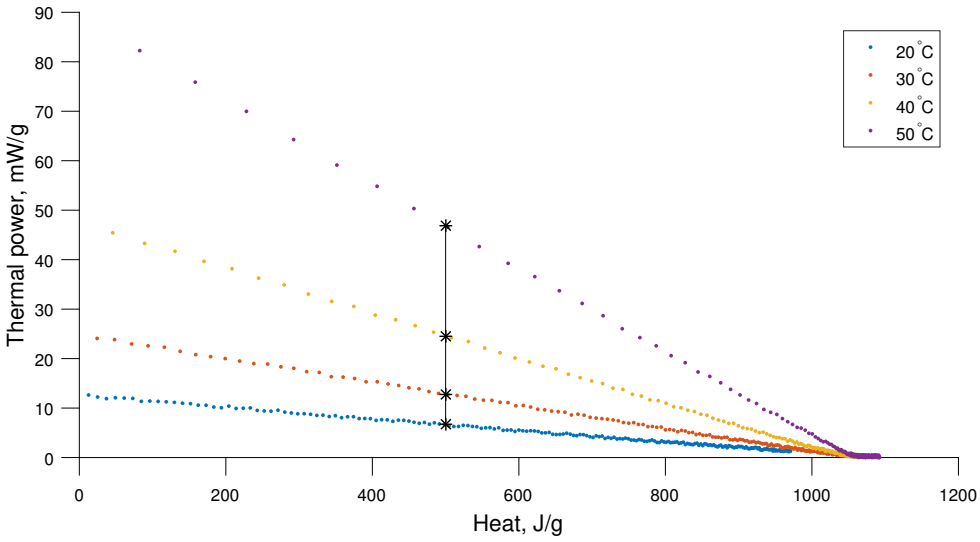

Figure 3.10: Extraction of thermal power $P(T, Q)$ in each isotherm

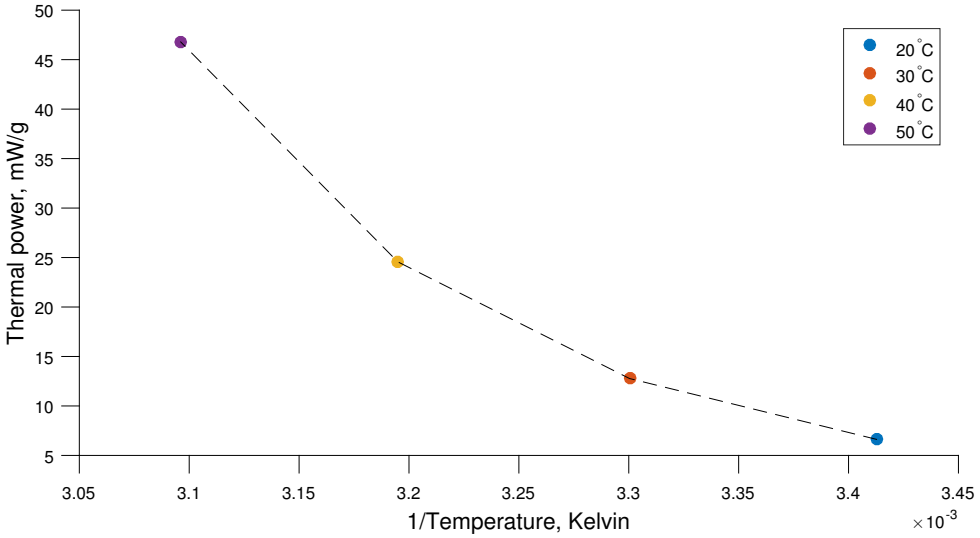

Figure 3.11: Extracted thermal power plotted against 1/T in the domain $P(1/T)$

In order to evaluate the thermal power for any other temperature that hasn't been measured, a logarithmic transformation of Eq. (3.11) will be used to evaluate the thermal power. The linear equation

$$\ln(P) = \ln(A) - \theta\frac{1}{T} \tag{3.12}$$

where

$$\theta = E/R \tag{3.13}$$

that is achieved after the transformation is very convenient, because it is possible to obtain the thermal power in each iteration using linear interpolation functions. The input parameter needed in the linear equation is the temperature of interest and gives the logarithm of the thermal power for a constant heat Q.

The linear relation that is obtained with use of Eq. (3.12) is illustrated in Figure 3.12. The thermal power is achieved by transforming the value back to the original domain $P(T, Q)$ with use of the exponential function.

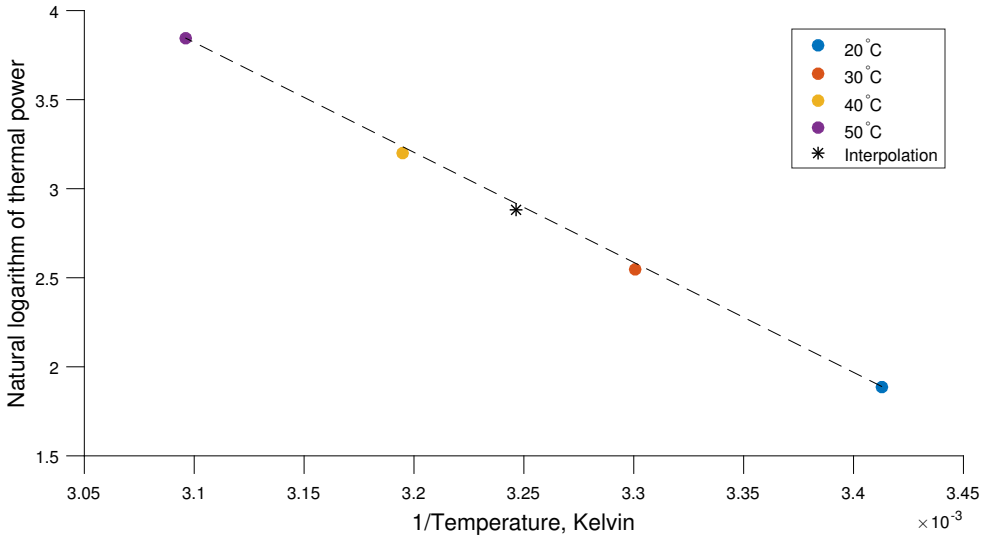

Figure 3.12: Linear relation in the logarithmic transformation

4 Algorithm

Most FEA programs for simulation of hardening concrete only have support for calculations based on the conventional method. The main objective in the dissertation was to develop tools for using data from isothermal calorimetric experiments in finite element programs. Two algorithms have been developed. One is a pre-processing part, developed in Matlab, which processes the data from the measurements to a data file, presented in Section 4.1. The second algorithm was developed to compute the thermal power of hydrating cement with use of isothermal calorimetric data and is presented in Section 4.2.

4.1 Processing of data

In Figure 4.14 a block diagram illustrates the steps involved in the processing of isothermal calorimetric data.

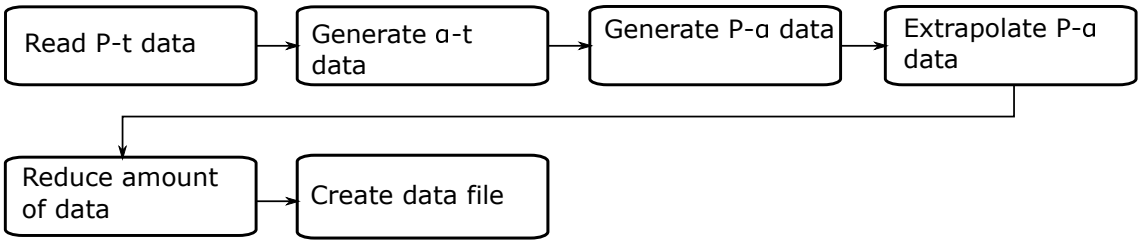

Figure 4.1: Steps when processing of data

4.1.1 Isoconversion of thermal power

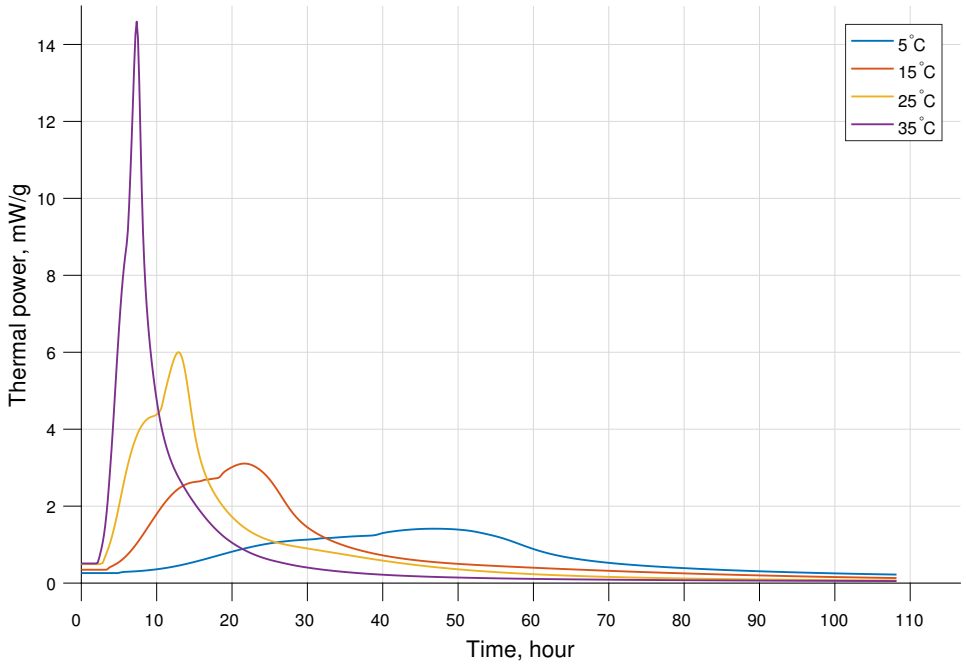

Figure 4.2: Schematic output from several isothermal runs in a heat conduction calorimeter of cement. Thermal power $P = P(t)$

The results of the cement hydration from the heat conduction calorimeter are the thermal power as a function of time, see Figure. 4.2, but is not the domain used for the application of isothermal measurements. As presented in section 3.3, the advantage of isothermal measurements is the possibility to express the thermal power to the degree of hydration α and temperature T.

The first step is to compute generated heat $Q(t)$ by integrating the thermal power according to Eq. (3.7). The integral is evaluated numerically as

$$Q(t) = \sum_{i=1}^{n(t)} P_i \Delta t \tag{4.1}$$

where P_i is the thermal power at recording no. i, Δt is the time interval between the recordings and $n(t)$ is the recording no. at time t.

The second step is to convert the heat to the degree of hydration α according to Eq. (2.8). For this procedure, the heat Q_∞ which corresponds to full hydration, is required. However, attaining Q_∞ is not trivial as most often calorimetric runs do not progress until Q_∞ is reached. The approach is therefore to estimate Q_∞. With knowledge of the composition of the cement, Q_∞ can be established. In Figure 4.3, the degree of hydration $\alpha(t)$ has been attained from the isothermal runs in Figure 4.2

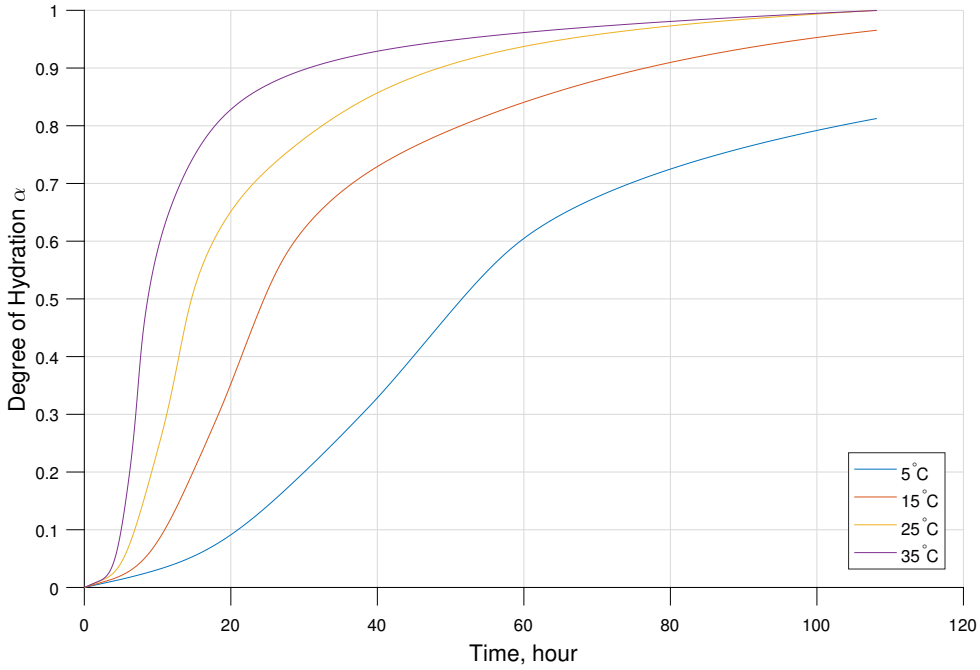

Figure 4.3: Degree of hydration with respect to time. Degree of hydration $\alpha = \alpha(t)$

In Figure 4.4, the thermal power $P(t)$ is plotted against the degree of hydration $\alpha(t)$. Hence, the thermal power P has been isoconverted and is evaluated as a function of α and T according to Eq. (3.10).

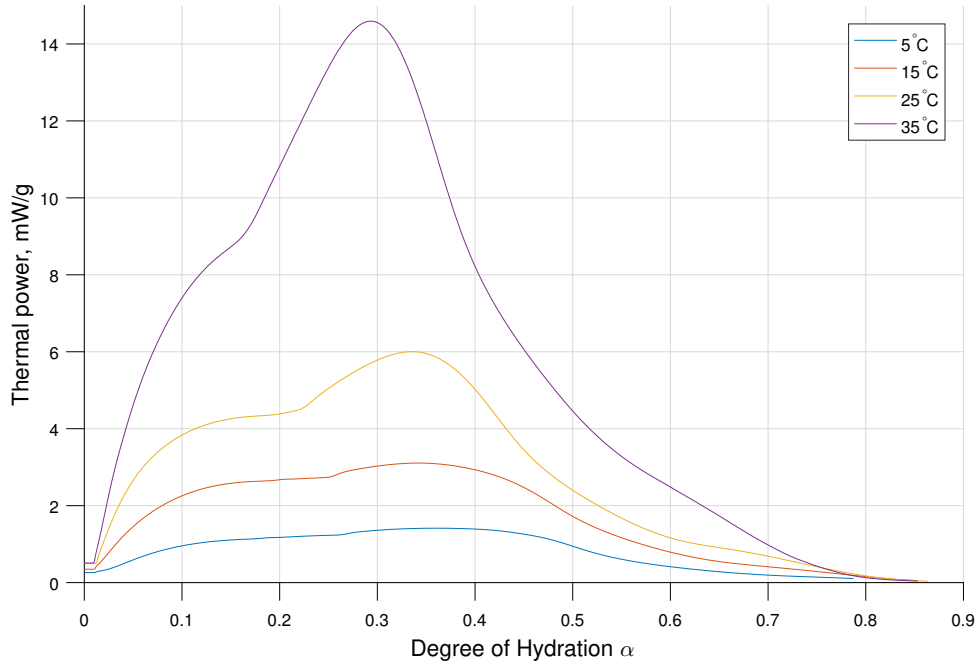

Figure 4.4: Isoconversion of the thermal power against degree of hydration. Thermal power $P = P(T, \alpha)$

4.1.2 Extrapolation

The advantage of the heat conduction calorimeter is that it captures the thermal power of the cement reaction with high accuracy in early periods. Generally, it isn't used for long term measurements, leading to insufficient data for long term simulations.

In Figure 4.5 the last part of the data in Figure. 4.4 has been enlarged and one issue can be observed. As each sample is ran at different temperatures the degree of hydration varies and it can be noted that the data sets do not end at the same degree of hydration. Therefore, if simulations progress for values of α where no data has been obtained, the issue is obvious that there's no data of the thermal power to the calculations, resulting in software issues. To avoid any issues regarding the software or other numerical issues, the solution can either be to limit the user to the length of time the simulation can proceed or it can be handled simply by extrapolating data with sufficient data points, anticipating that simulations won't be drawn-out as it's mostly the early ages that are of interest. Although an extrapolation part doesn't correspond to the true hydration, the second alternative is implemented in this project. This is however of limited influence as it affects the value of thermal power for high values of α, which is not of significance in simulations and for such values of α, the value of P is negligible.

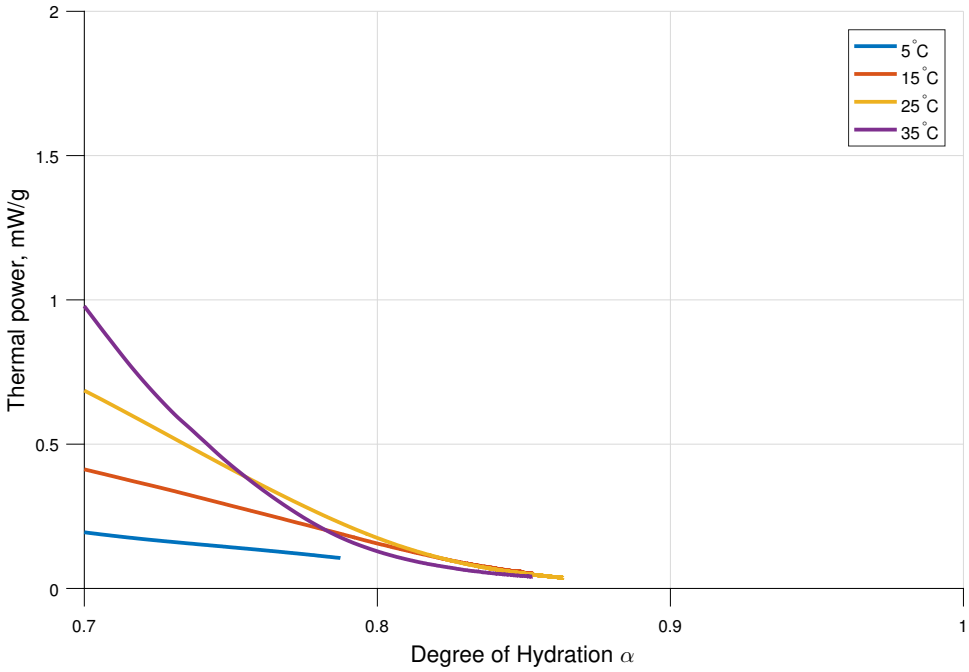

Figure 4.5: Enlarged view of the end of the data in Figure 4.4

When extrapolating the data, it's of interest to make a good model fit such that the extrapolated data follows same pattern as the measured data. From the measurements of the cement it is noted that the hydration proceeds in several periods and finding a model to fit the whole range of data becomes difficult. The extrapolation

data is therefore fitted to the latter part of the curves.

The model fitting is carried out by interpreting the last several hundreds of measurements as seen in Figure 4.5. However, the amount of data points used for the extrapolation should be dealt with individually for each measurement. From the data set it was noted that the thermal power showed tendencies of an exponential decreasing function, i.e

$$y = Ae^{Bx} \tag{4.2}$$

where A and B are fitting parameters.

Hence, a logarithmic transformation was performed to evaluate the fitting parameters and a linear regression was obtained by using the linear least square method of the data set. The equation

$$\ln(y) = \ln(A) + Bx \tag{4.3}$$

expresses the linear relation of the logarithmic transformation of Eq. (4.2).

In Figure 4.6 and 4.7, the last data points from an isotherm are presented and show varying noise, but still the overall data shows a good fit of a linear relationship in the logarithmic transformation. As illustrated by the solid line the trend appears to be a good fit but depending on the isotherm used, the error may increase as the data can be more noisy.

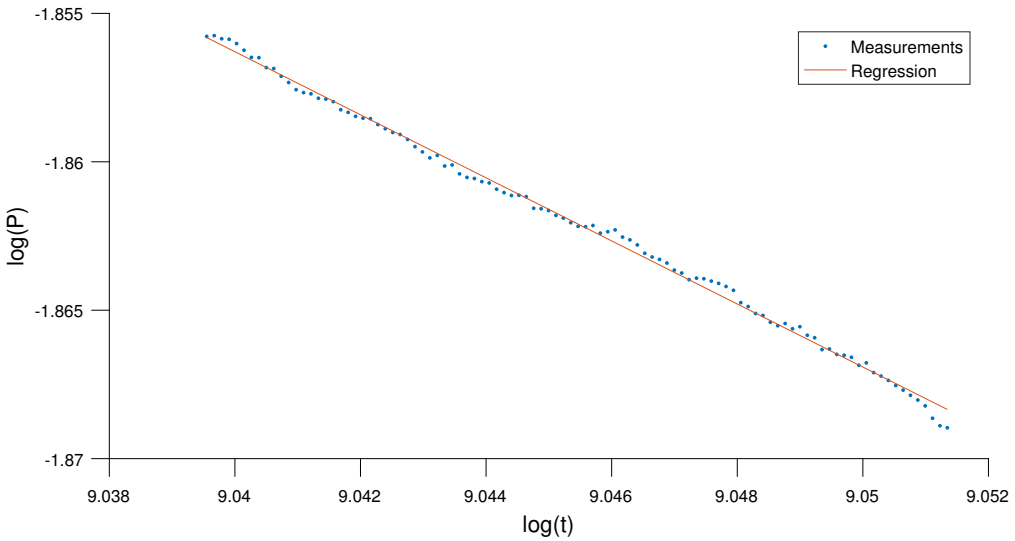

Figure 4.6: Regression of the last part of an isotherm in the logarithmic domain with little noise.

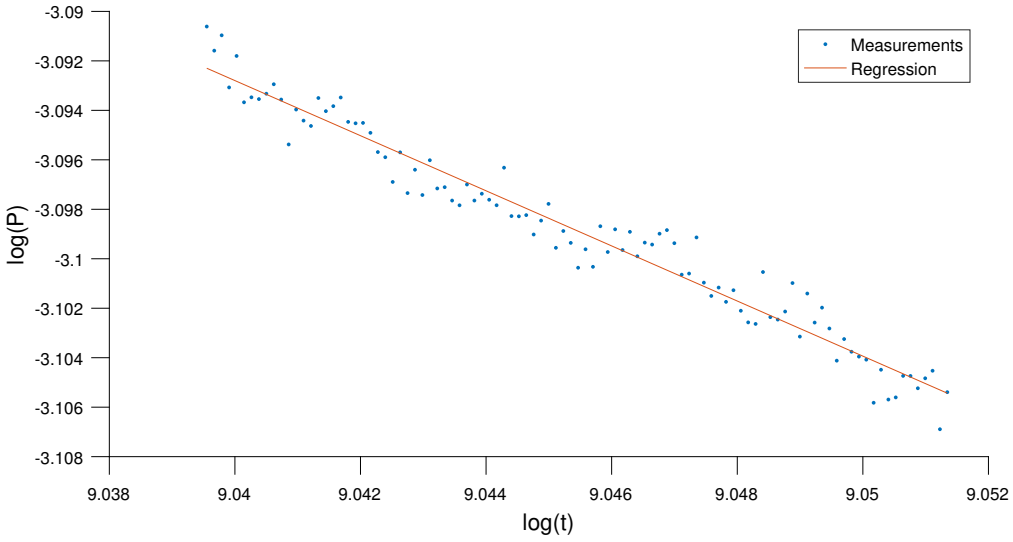

Figure 4.7: Regression of the last part of an isotherm in the logarithmic domain with more noise

As the linear relationship in the logarithmic transformation is obtained, the extrapolation is carried out to the original domain $P(T, \alpha)$ with the exponential function. Figure 4.8 illustrates the data set in the original domain, where transformation has been performed.

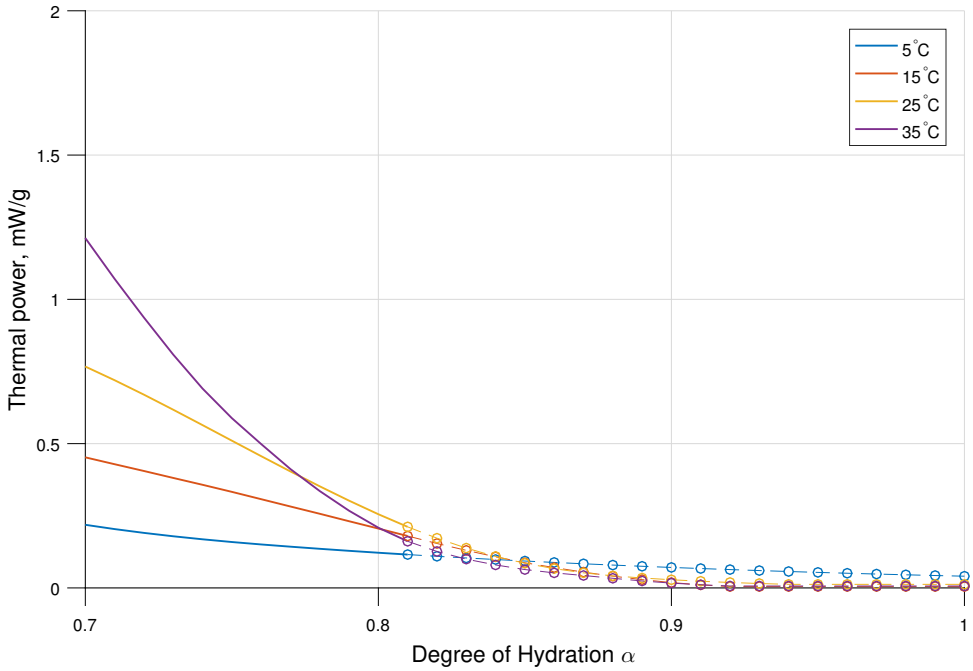

Figure 4.8: Extrapolation of the last part of the data in Figure 4.5 in the original domain $P(T, \alpha)$

4.1.3 File with calorimetric data

The received data from the calorimeter consists of usually more than several thousands of data points for each isotherm as data is recorded each minute and are often made at least during one week in order to capture the interesting periods of the hydration. However, it's not necessary to store data for each minute as the hydration of the cement mostly works in the unit of hours and as a consequence of large amount of data points, the numerical calculations become slower. By reducing the amount of data stored in the data file, the speed of the calculation can be improved as fewer data points need to be searched through in the algorithm. However, the reduction of data points has to be made with caution so that the accuracy of the curves isn't significantly disturbed. As shown in Figure 4.9 and 4.10 the data has been reduced from approximately 30000 to 101 data points, but the accuracy of the hydration is still preserved.

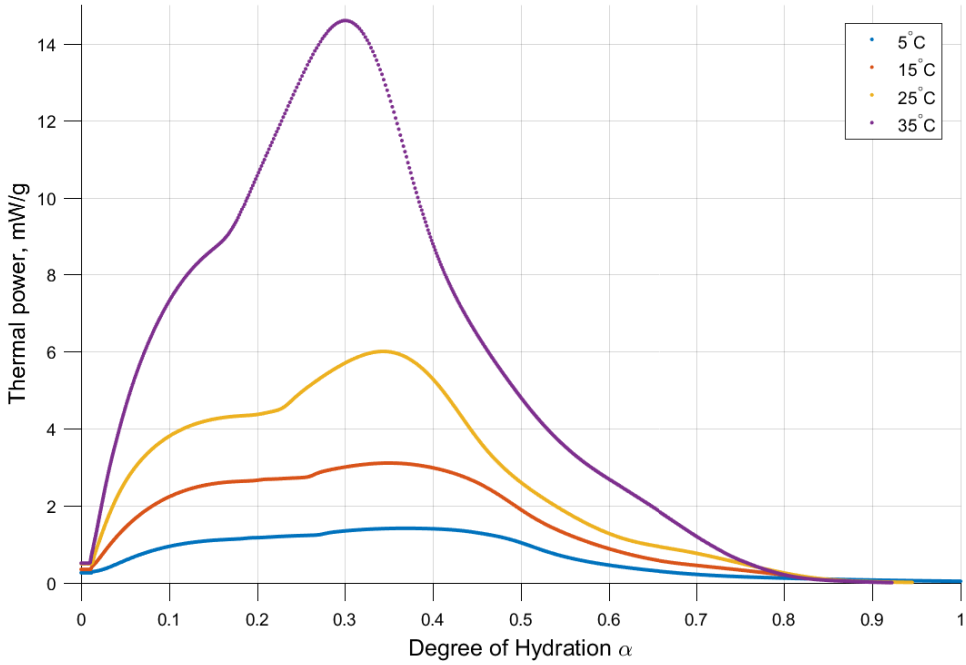

Figure 4.9: Unfiltered thermal power $P(T, \alpha)$ with approximately 30000 data points

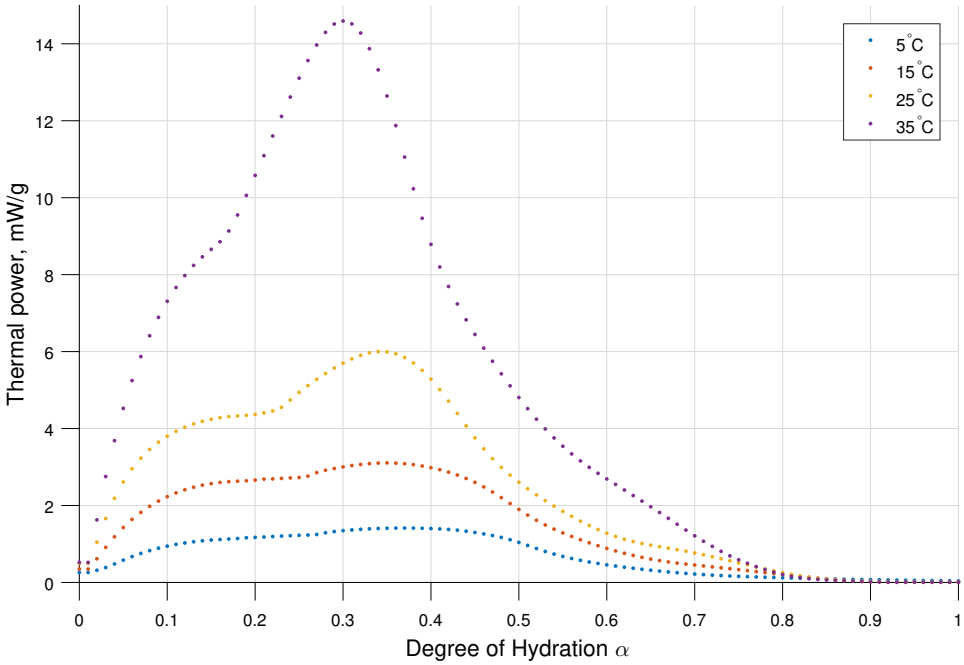

Figure 4.10: Filtered thermal power $P(T, \alpha)$ with 101 data points

As the data has been processed, the next step is to prepare the data for implementation into the simulation program. In order for the program to read the data correctly the input file needs to be set up in a particular structure which is obtained by organising a .txt file according to Table 4.1. Subsequently as the data is organised correctly, a conversion to .hcv needs to be performed and is simply made by changing the file extension .txt to .hcv.

Table 4.1: Structure of the data file

[n]	[m]		$[Q_\infty]$
$[T_1]$	$[T_2]$	...	$[T_n]$
[Data of isotherm T_1]	[Data of isotherm T_2]	...	[Data of isotherm T_n]

- Row 1: Contains information of the dimensions of the data. The first value is number of data points n in each isotherm and the second value specifies the number of columns n, where each column is data for one isotherm. The last value specifies the ultimate heat Q_∞ in [J/kg].
- Row 2: Specifies the isotherms in °C.
- Row 3 to n+2: Value of the thermal power $P(T, \alpha)$ for $\alpha = 0$ to $\alpha = 1$ at equal intervals.

Table 4.2 is an example of the layout in the file.

Table 4.2: Example of the file with calorimetric data

101	4	328000	
5	15	25	35
0.24675579	0.37269395	0.49094919	0.74346921
0.24675579	0.37269395	0.49094919	0.74346921
0.28115291	0.42976449	0.64440554	0.75336057
0.38767262	0.63811529	1.02403985	1.35244153
0.51309805	0.86537093	1.44238320	2.01162005
0.64303683	1.09175095	1.82960043	2.64270331
0.76577793	1.29802167	2.17621545	3.20549788
.	.	.	.
.	.	.	.
.	.	.	.
.	.	.	.
0.00000000	0.00000000	0.00000000	0.00000000

4.2 Isoconversional method - Computation of thermal power

The second algorithm, which is used for computing the thermal power was developed in the program language Fortran 95 with use of Microsoft Visual Studio. In this section the algorithm that uses the data for the calculations is presented and the procedure can be illustrated as in Figure 4.11.

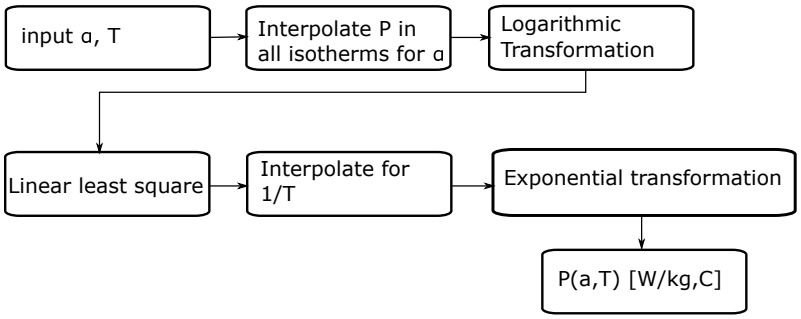

Figure 4.11: Procedure of computing thermal power

To solve the initial value problem, as presented in Section 4.3, the procedure is to solve the equations in time steps. In each time step of the transient problem, the temperature and the degree of hydration are obtained in the previous time step. In step 1, see Figure. 4.11, these variables are used as input parameters to the second step. With the input parameters known, the thermal power can then be extracted from the isothermal data, see Figure 4.12, re-emphasising that the thermal power according to Eq.(3.10) is a function of temperature and the degree of hydration. The figure simulates a fictitious time step t_n where the degree of hydration is the input parameter and illustrates that for a certain α, thermal power is extracted from each

isotherm.

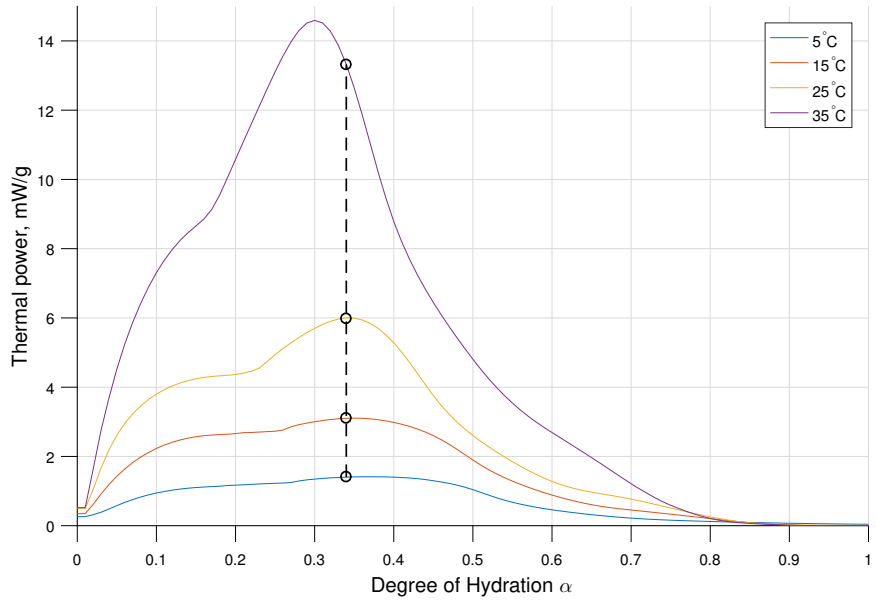

Figure 4.12: Extraction of thermal power $P(T_i, \alpha)$ in each isotherm

With use of Eq. (3.12), the third step is to transform the extracted thermal powers to a logarithmic domain, shown in Figure. 4.13 where a linear relation can be observed, which is obtained with the linear least square method. The temperature established in the previous iteration step is used as the input parameter. The logarithm of the thermal power is obtained on the regression line with the inverse of the temperature $(1/T)$, in Kelvin.

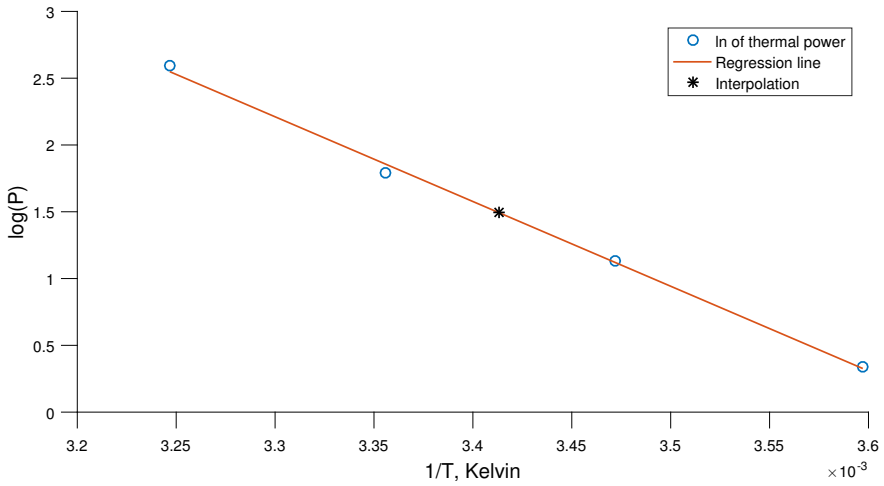

Figure 4.13: Thermal power in the logarithmic domain

The thermal power is then transformed to the original domain $P(T, \alpha)$ using the exponential function as seen in Figure. 4.14

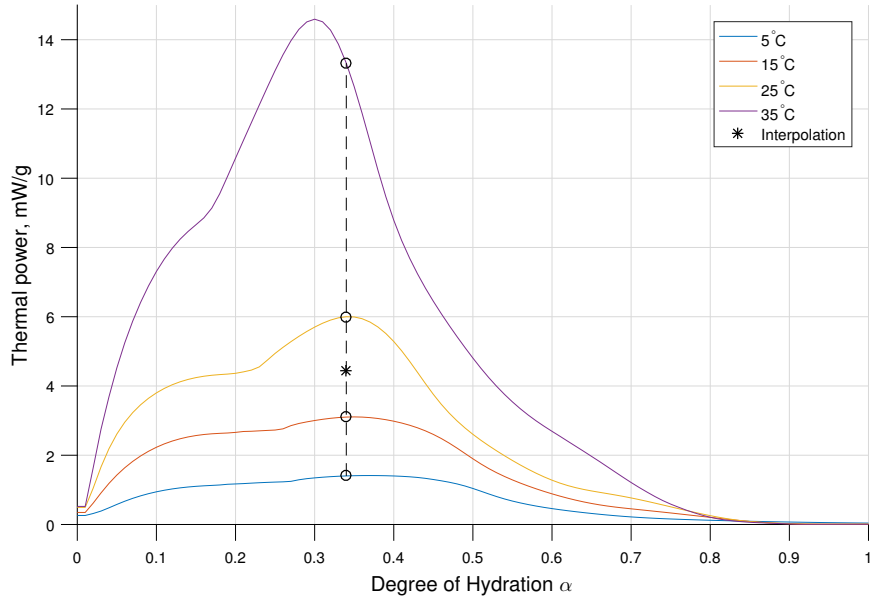

Figure 4.14: Interpolated thermal power $P(T, \alpha)$ in original domain

In Appendix C a study of the linear relation of the temperatures for different degree of hydration was performed which showed quite good linearity in the interval of $\alpha = 0.0$ and $\alpha = 0.7$. A second algorithm was also developed but with use of simple linear interpolation to examine how different interpolation methods influenced the results. The differences of the results between the two interpolation methods were minimal, see Appendix D.

4.3 Finite element simulation of hardening concrete

The finite element method is a numerical approach of solving differential equations describing physical problems. The differential equations are assumed to describe a variable, e.g. temperature, over a finite region. Within an element, nodal points are located where the studied variable is computed and between the nodal points, the approximation of the variable is a polynomial interpolation. This is a characteristic feature of the finite element method that approximates the differential equation in small regions (finite elements), instead of finding an equation that holds for the entire region. Therefore, with the finite element method applied, solutions for a non-linear dependence of a larger region is obtainable by simple approximations on small elements. Further, using specific rules, the elements are assembled together to form the entire region.

In Figure 4.15 an illustration of the simulation procedure is presented. The first step is to interpret the physical phenomenon of the domain and choose the type of analysis to be made, e.g. stress analysis, heat conduction analysis or fluid dynamic

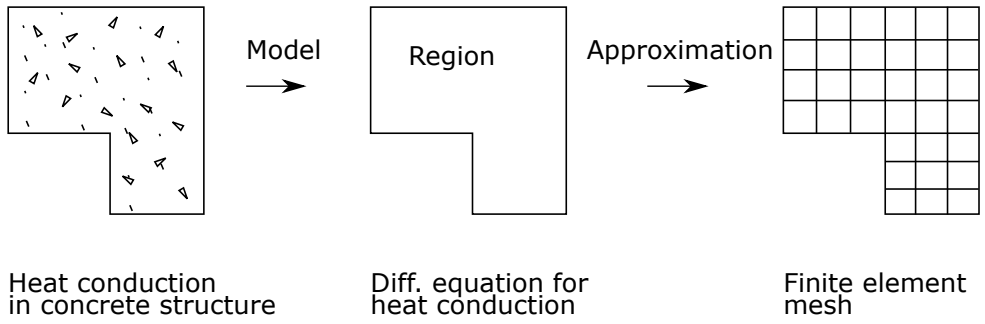

Figure 4.15: Illustration of modelling steps of a simulation with finite element analysis

analysis. The image to the left-hand side illustrates the domain for a concrete structure where heat conduction analysis is to be performed. The second step is to define the region and the boundary of the domain and subsequently choose the differential equation used for heat conduction. Fourier's law is used for thermal transfer, which is given in differential form by

$$q_i = -k\frac{\partial T}{\partial x_i} \tag{4.4}$$

where

k is the thermal conductivity of the concrete,

T is the temperature,

x_i are Cartesian coordinates.

The third step is to divide the domain into finite elements as seen in Figure 4.15 and solve the partial differential equation in Eq. (4.5) in each element to obtain the variation of temperature.

$$\frac{\partial q_i}{\partial x_i} + \rho c\dot{T} - \Theta = 0 \tag{4.5}$$

where

q_i is the heat flow vector in Eq. (4.4)

c is the specific heat capacity

ρ is the mass density,

$\Theta = \Theta(t)$ is the internal generated heat,

In the computer program, the partial differential equation in Eq. (4.5) is solved by a finite element formulation

$$K_{mn}a_n + C_{mn}\dot{a}_n = f_m \tag{4.6}$$

which is achieved by formulating a weak formulation of Eq. (4.5) and with use of the Galerkin method [35], the finite element formulation is expressed as

$$K_{mn} = \int_V \frac{\partial N_m}{\partial x_i} k \frac{\partial N_n}{\partial x_i} \mathrm{d}V \tag{4.7}$$

$$C_{mn} = \int_V N_m \rho c N_n \mathrm{d}V \tag{4.8}$$

$$f_m = \int_S N_m q_n \mathrm{d}S + \int_V N_m \Theta \mathrm{d}V \tag{4.9}$$

where the heat Θ is computed as

$$\Theta = P D_{cem} \tag{4.10}$$

where

D_{cem} is the amount of cement kg/m^3

$P = \dot{\Theta}$ is conventionally computed using Eq. (2.10). Using data from isothermal calorimetry it is instead obtained with the algorithm described in Section 4.2.

The nodal temperatures are computed by solving Eq. (4.6) using a time stepping procedure.

5 Experiment and simulation

In this project a setup was built to examine how well a FEA program with different calculations of the generated heat estimates temperatures within a hardening concrete structure. The FEA program that was used is HACON. Previously, the calculation of the thermal power in HACON was computed as the time derivative of Eq. 2.10 but now, it also has support for isoconversional calculation according to Section 4.2.

This chapter presents results from the experiment and simulations with the updated version of HACON. If the reader is interested in the algorithm then further analysis of the implementation is described in the Appendices.

5.1 Results from heat conduction calorimeter

The thermal power for each isotherm in the $P(T, \alpha)$ domain, as seen in Figure 4.10, are unique for each concrete or cement type. Therefore, isothermal measurements were performed for the same concrete that were cast in the experimental setup, described in Section 5.2. The procedures made to obtain the results from the isothermal measurements will be presented in this section and subsequently, the results will be used in the simulation of the setup, described in Section 5.3.

When the isothermal measurements are performed, certain procedures need to be made in order to attain good results. A disadvantage of the heat conduction calorimeter is that it measures only small samples. Hence, large aggregates need to be removed for measurements of concrete in order to measure the heat properly.

When the concrete was mixed, part of it was carried over to a sink to sieve out aggregates of large sizes. As the concrete was sieved and consisted of only smaller aggregates, the vessels in the calorimeter were filled to approximately 25% of the total volume to accommodate adequate heat flow.

The output from the calorimeter is the total thermal power of the sample, however, it's more convenient to evaluate the results in terms of thermal power per cement mass (mW/g), which requires the mass of cement in the vessels to be established. Therefore, evaluation of the amount of cement in the samples was performed by Flemark [1]. In Figure 5.1, results from the heat conduction calorimeter are pre-

sented, where the measurements of the thermal power were performed in isotherms of 5, 12, 20, 27, 35 and 50 °C. Processing the experimental data according to the desciption in Section 4.1 assuming $Q_\infty = 328000$ J/kg the relations between thermal power P and degree of hydration α illustrated in Figure 5.2 where obtained.

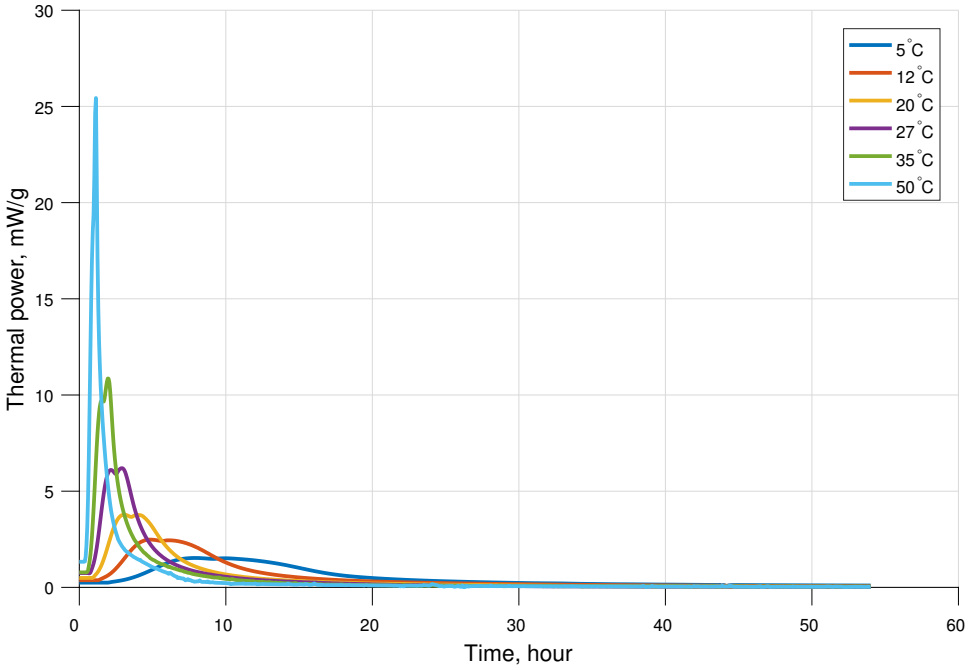

Figure 5.1: Results of the thermal power $P(t)$ from the heat conduction calorimeter for the cement used in the experimental setup.

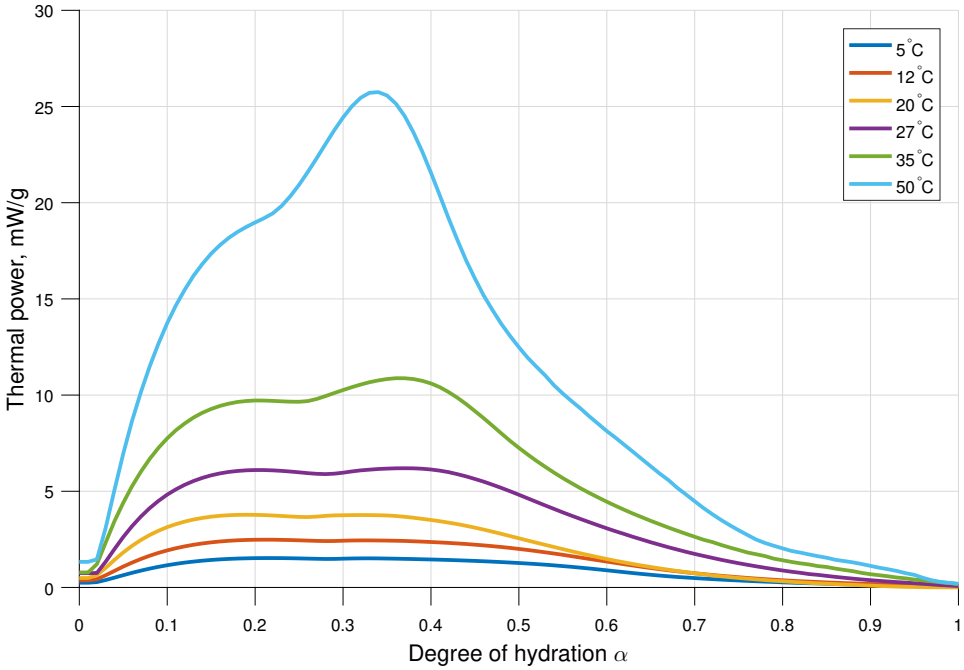

Figure 5.2: Isoconversion of the thermal power $P(T, \alpha)$

5.2 Experiment

Preliminary simulations were performed in order to build a setup such that two dimensional heat flow occurs. Hence, several simulations with different geometries and boundary conditions were tested to find a setup that was simple to build, but still obtained a 2D-heat flow. The factors that came into mind when determining the setup were also to build it such that the maximum temperature was high and the difference between the minimum and maximum temperature in the body was high. Finally, after several runs considering the mentioned aspects, the setup was determined in accordance to Figure. 5.3. After the setup was built, the simulations were refined to match final material parameters and boundary conditions of the setup. Measurements were provided for 21 points of the setup but only point no. 1, 12, 19 and 22 will be presented due to the large amount of data. Subsequently these points will be compared with the same positions in the simulations.

5.2.1 Experimental setup

The setup was built by Flemark [1] and was cast in laboratory as the environmental conditions are controlled, thus, the boundary conditions in the simulation model are set with high accuracy. If the casting would have been performed in exterior climate, the boundary conditions of the model would become harder to determine as the temperature and humidity may fluctuate. The casting was performed at the

Division of Building Materials at LTH, Lund University. This section presents the cast concrete, of which the purpose is to have a reference setup to the simulation model.

The form was made of a pipe in PVC and was partly surrounded by EPS insulation, see Fig 5.3. In the setup 21 thermocouples were placed along the height of the pipe and spread out outwards from the symmetryline of the pipe to the edge and 3 thermocouples were placed outside the setup to measure the air temperature, see Fig 5.3. In order to maintain the boundary conditions of the model in the experimental setup, a fan was installed approximately 1 meter away from the pipe to prevent any temperature rise close to the pipe due to the heat flow going out of the setup, see 5.4.

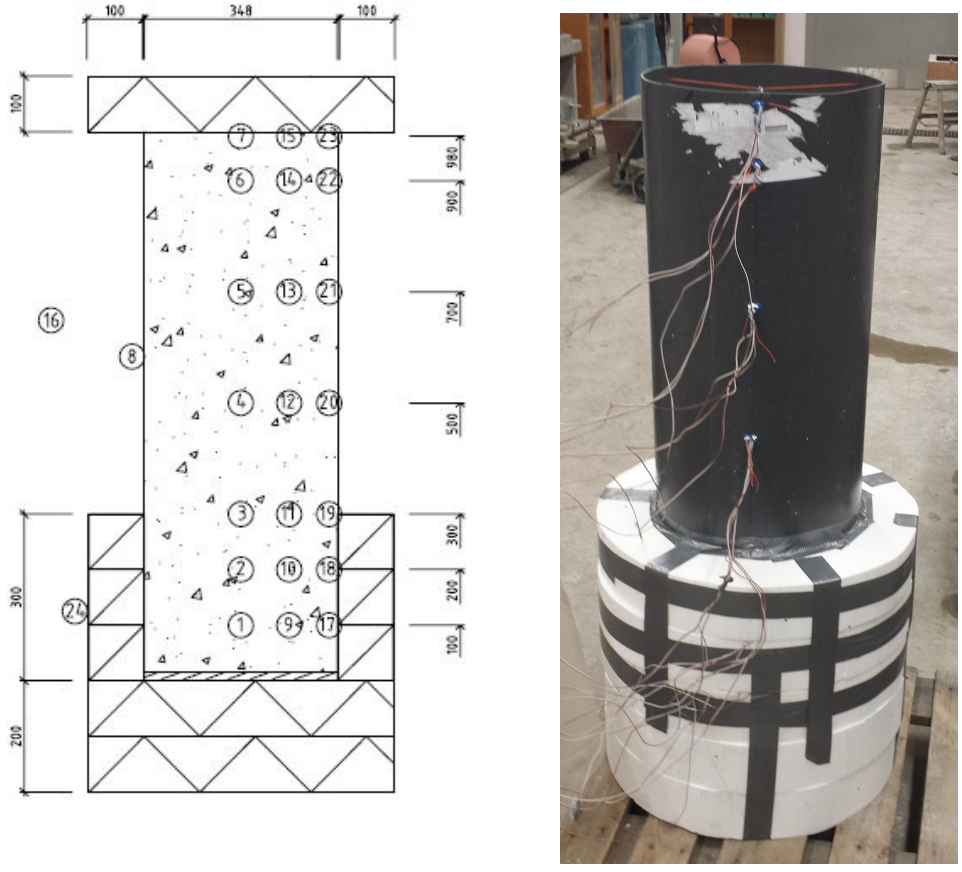

(a) Drawing of the setup where the numbers represents each thermocouple

(b) Experimental setup

Figure 5.3: Experimental setup

Figure 5.4: Setup of the experiment

As the setup included 24 thermocouples, a lot of data has been received, however, in order to keep down the amount of results in this chapter, only 4 thermocouples will be extracted and compared to the simulations.

In order to examine the hottest part of the casting, thermocouple 1 was chosen as the placement of the thermocouple is at the symmetry line and close to the insulation in the bottom.

Three thermocouples were aligned where the insulation in the bottom ends. Thermocouple 19 is closest to the boundary and was chosen to be studied, as much of the heat flow dissipates through this thermocouple.

In the upper part of the casting, much of the heat flow was expected to occur along the pipe. Therefore, results from thermocouple 22 is extracted.

The results from each method used in the simulations are presented in Section 5.3.1 and Section 5.3.2.

5.2.2 Results from experiment

The measured temperatures from the setup are presented in Figure. 5.5 for thermocouple 1, 12, 19 and 22. As expected, the thermocouples (1 and 19) close to the insulation at the bottom show higher temperatures than the thermocouples (12 and 22) away from the bottom insulation.

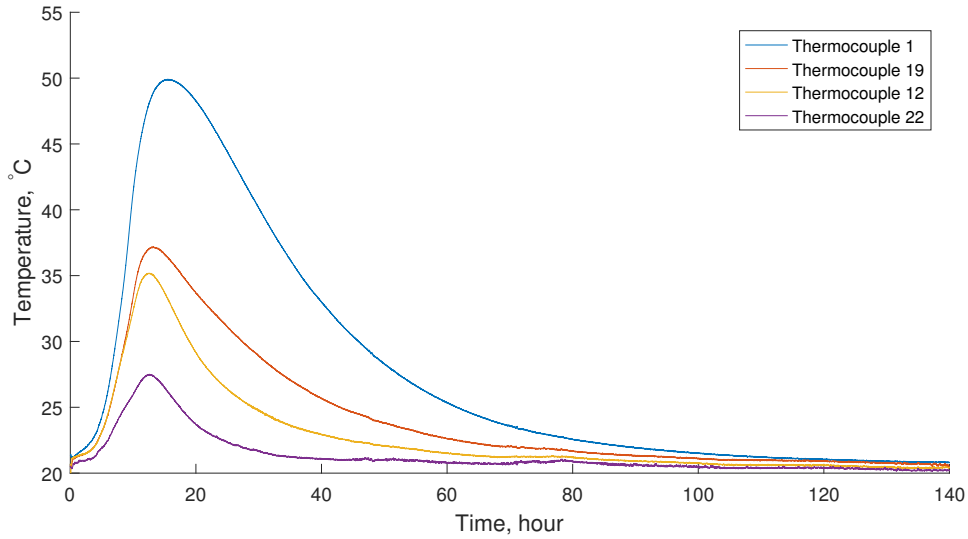

Figure 5.5: Temperature development from the experimental setup in thermocouple 1, 12, 19 and 22

5.3 Simulation

Two different simulations of the setup were performed. One simulation was performed with the conventional method. The other simulation was performed with the developed algorithm, based on the isoconversional method.

The modelling in the simulation step was carried out rather simply as the experimental setup was built axisymmetric. The model in Figure 5.6 illustrates the axisymmetric geometry and the dimensions of the model are presented in Table 5.1. The model consists of 2 surfaces where each surface is set with the properties according to Table 5.1-5.3. The elements are made approximately quadratic and the surfaces are represented by segment 1-4 and 4-7 respectively. The material parameters of the concrete in Table 5.3 set in accordance to ”Byggcement, recept nr 2” in reference [36]. The simulation was performed for a time of 168 hours = 1 week to observe the early age heat developments in the model. Simulation longer than 1 week wasn't necessary, as the temperatures acclimatised with the boundary conditions within a few days. The boundary conditions applied on the model consisted of different types of isolating materials, details are shown in table 5.2.

Due to the asymmetric air flow produced from the fan, it became hard to make an accurate model of the wind in the simulation as only 2D and axisymmetric modelling was supported in HACON. Anyhow, the approach was to assume a symmetric wind velocity for the model. However, the wind velocity couldn't be provided by measurements. Hence, an estimation of the wind velocity was performed by a parametric study of the wind velocity until good agreement between the temperature computed using the conventional method and the temperatures measured in the experiment was obtained. The wind velocity was adjusted in the simulation with the conventional method so that the maximum temperature in the position of thermocouple 2, 5 and 22 were close to the maximum temperature within a range of -3 to +3 °C to the corresponding thermocouple. The procedure was successful as it was possible to find a good fit by adjusting only the wind velocity. The same wind velocity was then applied to the model with the isoconversional method.

However, it will not be possible to validate the accuracy of the simulations to the measurements, as the wind velocity isn't quantitatively attained. But it is still possible to observe the differences between the methods, as the simulations are performed with the same conditions.

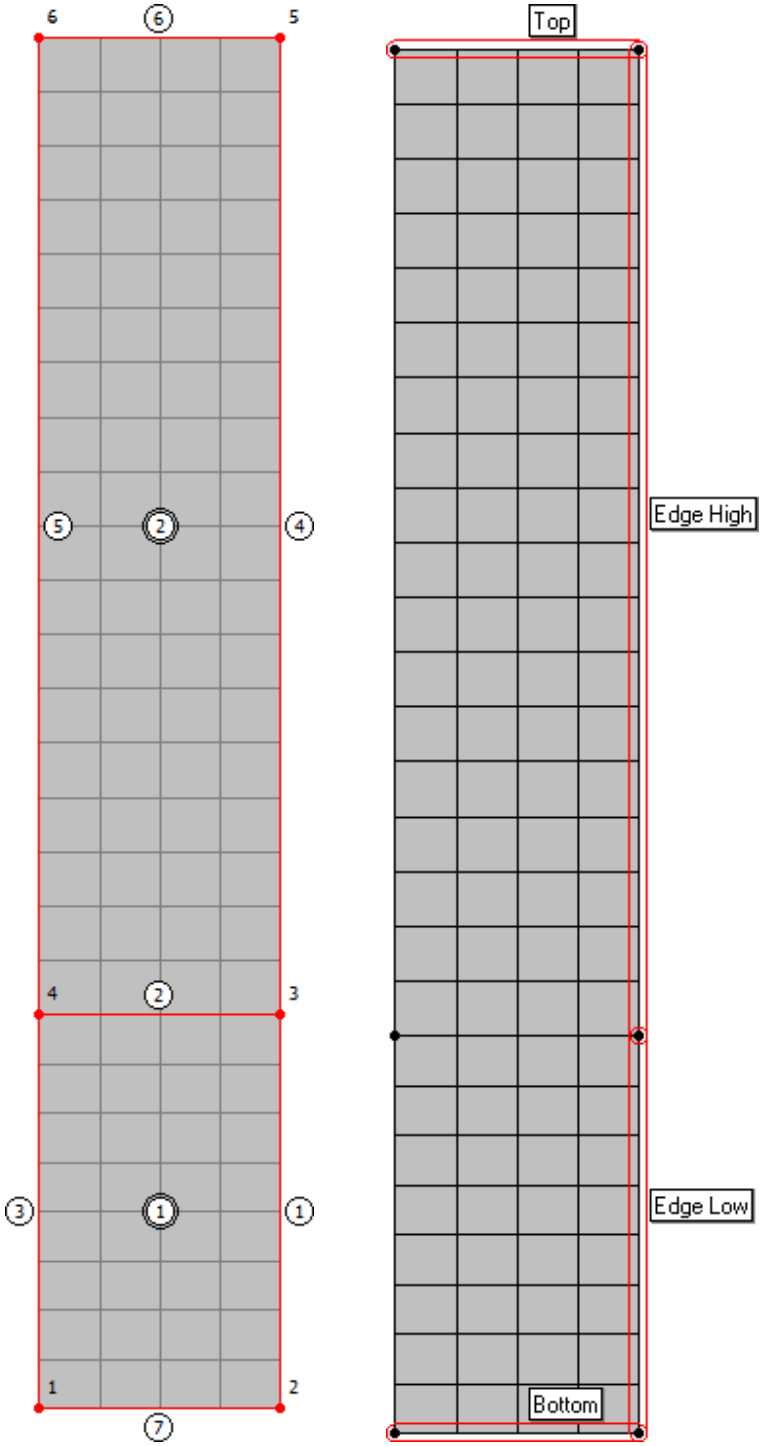

(a) Geometry and mesh of the model

(b) Boundary conditions applied on the model

Figure 5.6: Model of the setup in HACON.

Table 5.1: Model specifications

	Surface 1	Surface 2
material	Bas Cement S4	Bas Cement S4
height	284	704
width	174	174
segments	1-4	4-7
mesh, no. of rows	8	18
mesh, no. of columns	4	4
boundary conditions	"Bottom" + "Top"	"Edge Low" + "Edge High"

Table 5.2: Specification of Boundary condition

	"Top"	"Edge High"	"Edge Low"	"Bottom"
Material	EPS	PVC	EPS	EPS
Thickness, mm	100	3.5	100	200
Thermal cond., W/m,K	0.029	0.16	0.029	0.029
Wind velocity, m/s	1.0	6.0	1.0	1.0
Initial temperature, °C	20.92	20.92	20.92	20.92
Avg. temperature, °C	20.10	20.10	20.10	20.10

Table 5.3: Material specification

BasCem S4					
Parameters of Eq. (2.10) [36]		Parameters of Eq. (2.6) [36]		Material Parameters of the concrete	
λ_1	1.00	θ_0	2715	Density, kg/m^3	2398
t_1	6.55	κ_0	0.00	Final heat, J/kg	328000
κ_1	2.18			Cement content, kg/m^3	350
				Eqv. w/c-ratio	0.55
				D_{max}	16
				Thermal cond., W/m, K	2.189
				Specific heat, J/kg, K	873

The simulations were performed with the conventional method and isoconversion method. Subsequently the results were obtained and transferred into Matlab in order to generate plots of the results.

5.3.1 Result from simulation with conventional method

Figure 5.7 presents results from the simulations in HACON with use of the conventional method, where the fitting parameters in Eq. (2.10) are set in accordance to table 5.3. The temperature development is extracted for the position of thermocouple 1, 12, 19 and 22 in the simulation model.

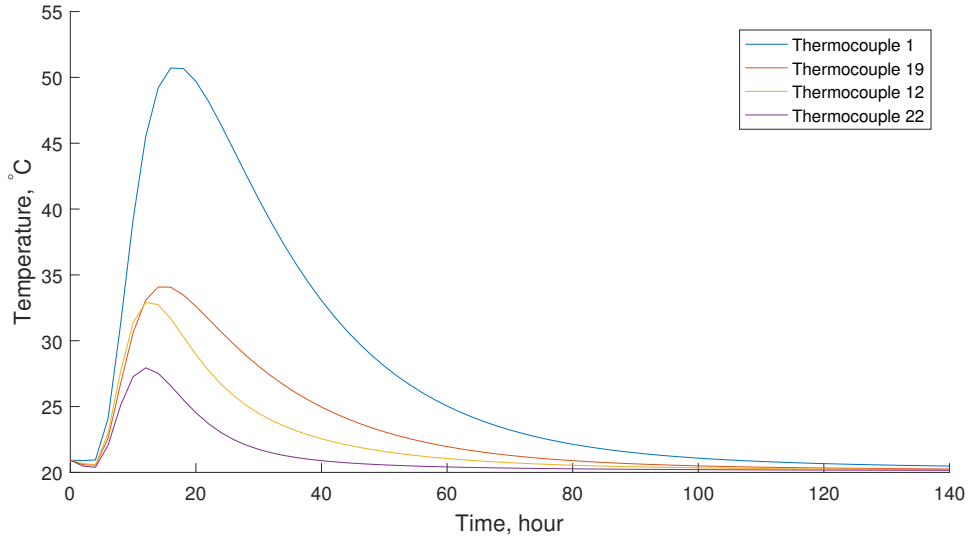

Figure 5.7: Temperature development in the position of thermocouple 1, 12, 19 and 22 with conventional method

5.3.2 Result from simulation with isoconversional method

An input data file was created for the measurements from the heat conduction calorimeter in Figure. 5.2 and was implemented to the updated version of HACON. Figure 5.8 presents the results from simulation with isoconversional method. The temperature development is extracted for the position of thermocouple 1, 12, 19 and 22 in the simulation model.

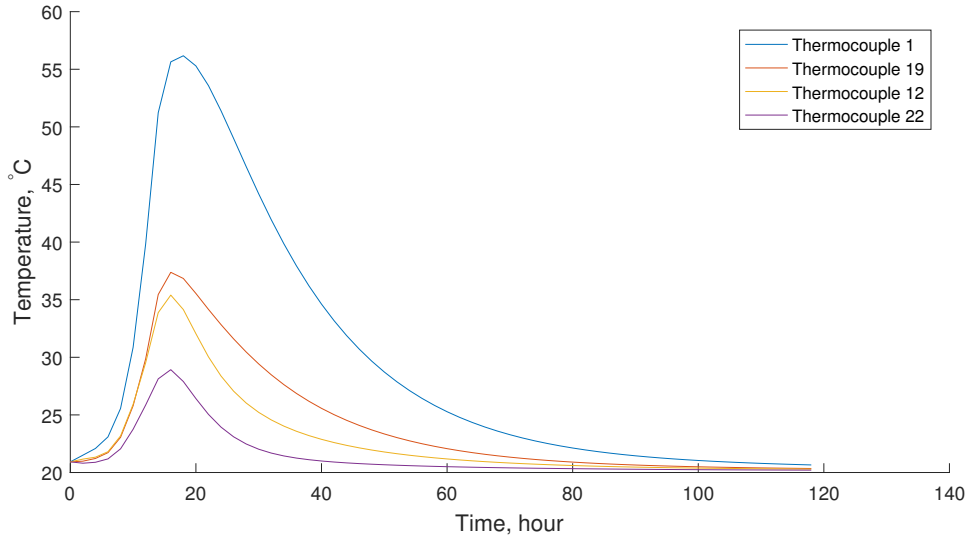

Figure 5.8: Temperature development in the position of thermocouple 1, 12, 19 and 22 with isoconversional method

5.4 Comparison

In this section, temperature distribution and temperature development from the experimental setup and the simulations will be compared.

5.4.1 Temperature distribution of the setup

With the data from the thermocouples, a meshgeneration of the temperature in the setup was made to visualise the temperature distribution. It can be observed in Figure. 5.9 how the temperature distribution has developed at 6, 10, 16, 22, 26 and 36 hours.

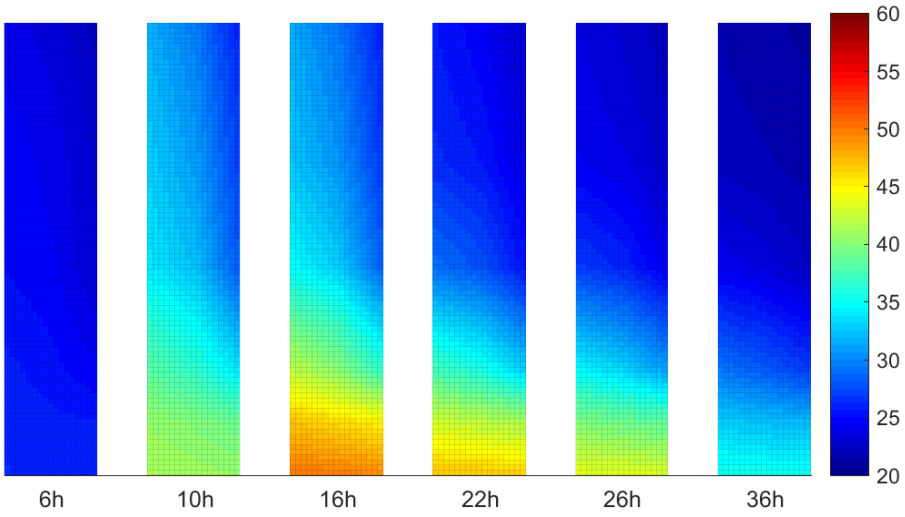

Figure 5.9: Temperature evolution of the setup from the experiment

Likewise, the temperatures from the conventional and isoconversional method were visualised, see Figure. 5.10 and 5.11. It can be observed that the temperature distribution in the simulation models showed good agreement with the gradients in the setup. With use of the isoconversional method, the temperatures are generally lower than in the conventional method until 10 hours but at 16 hours the temperatures are generally higher and remains higher until 36 hours.

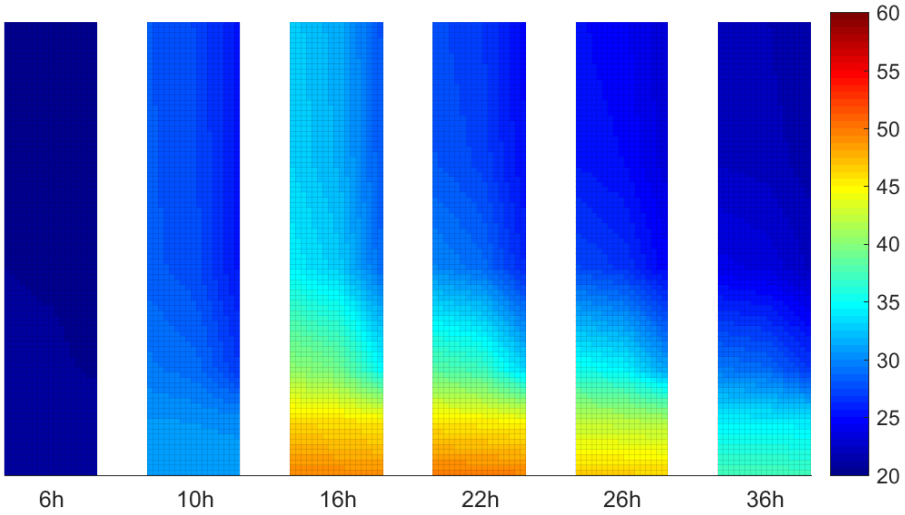

Figure 5.10: Temperature evolution of setup from heat calculations based on the conventional method

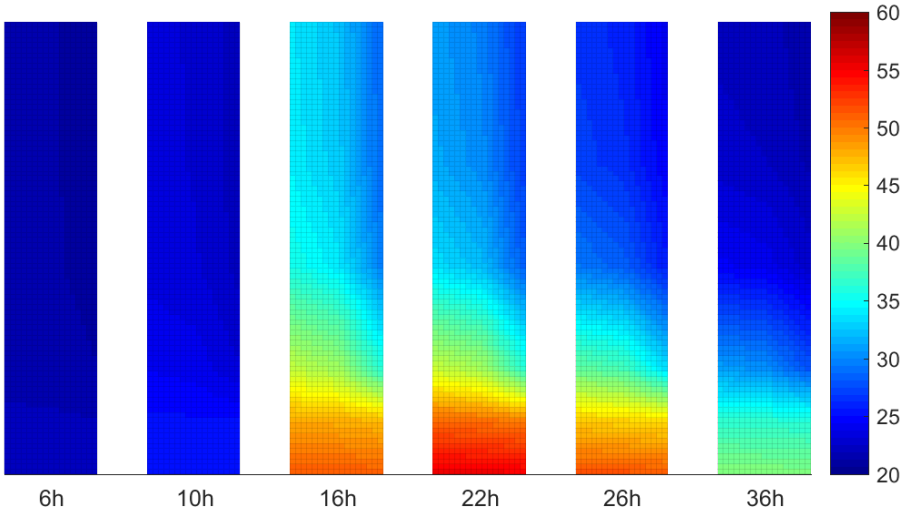

Figure 5.11: Temperature evolution of setup from heat calculations based on the isoconversional method

5.4.2 Deviation of maximum simulated temperature from the measurements

As the conventional method was fitted to the measurements it was expected that the temperatures from the simulation would show good agreement. With the same conditions applied for the isoconversional method, it was interesting to observe how well the simulations estimated the maximum temperature in the entire setup. This was made by calculating the maximum temperature in the position of the thermocouples for each simulation and subtract the maximum temperature from the corresponding thermocouple. The objective was to visualise how much the maximum temperature in the model diverged from the setup. The visualisation was made by making a mesh of the differences in absolute value for the setup, see Figure. 5.12.

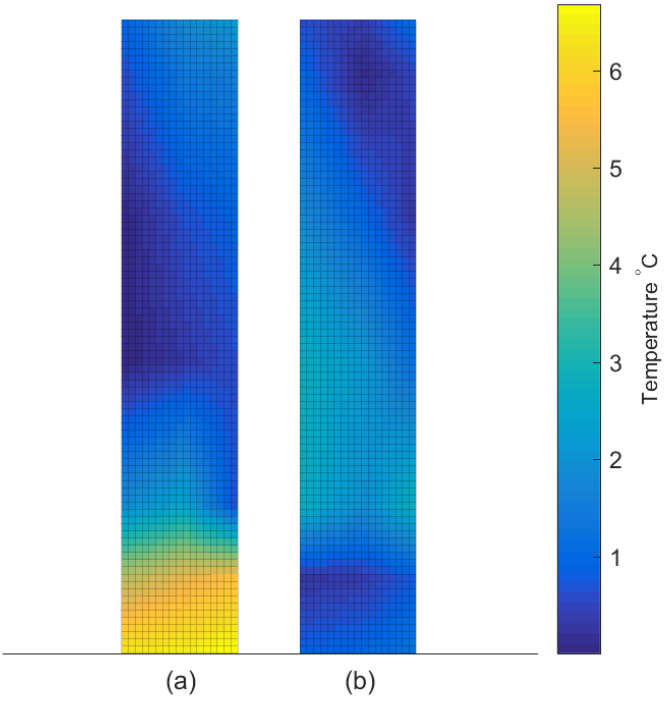

Figure 5.12: Deviation of the maximum temperature in °C from the simulations compared to the measurements. (a) Isoconversional. (b) Conventional.

It can be observed that the simulation with the conventional method shows quite good agreement with the measurements, with just few degrees differences in the entire setup. However, the isoconversional method shows more divergence from the measurements in the lower part of the setup, where the differences reach up to 6 °C. For the upper part of the setup, the simulations show similar results as the conventional method.

However, note that the wind velocity in the model was estimated from the simulation and the intention of the results are not to be interpreted as which model is more

accurate. What is observed is that the different methods estimate the maximum temperatures differently.

5.4.3 Comparison of temperature development

As the simulations were performed with different formulations of the heat development, it is of interest to contrast the results from each other. In Figure 5.13-5.16, the results for the different methods are compared with each other and with the measurements. With the same conditions applied for the simulations, it can be noted that the results of the temperature developments are slightly different.

In the position of thermocouple 1 it is noted that the isoconversional method shows a slight delay in the acceleration period but reaches higher temperatures than the measurements and the conventional method at approximately 20 hours. The conventional method estimates the temperature very well. In later periods both methods estimate the temperature equally well.

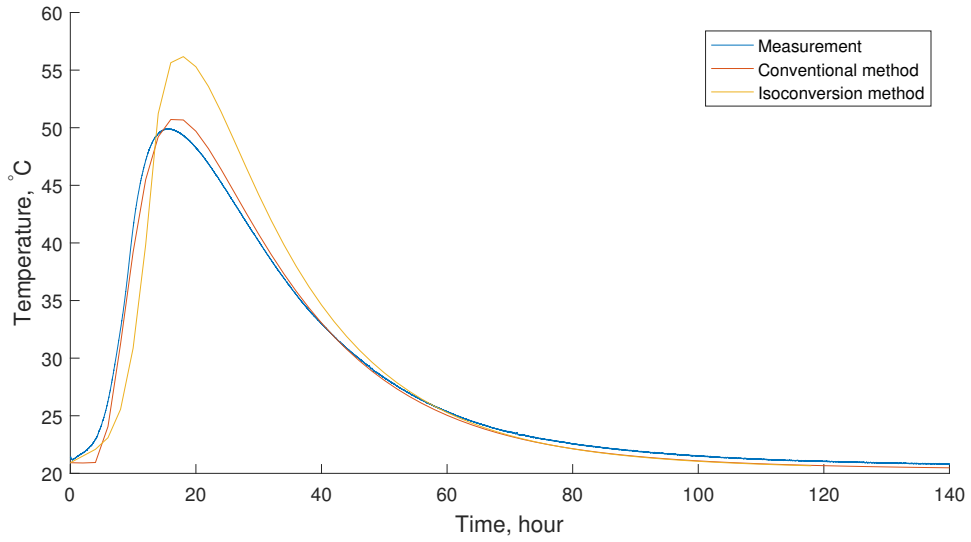

Figure 5.13: Temperature at position of thermocouple 1 from measurements and calculations with conventional- and isoconversional method

In the position of thermocouple 12 and 19, the differences are reversed where the isoconversional method fits the temperature better but delayed. The conventional method underestimates the maximum temperature but the time when it occurs is well estimated.

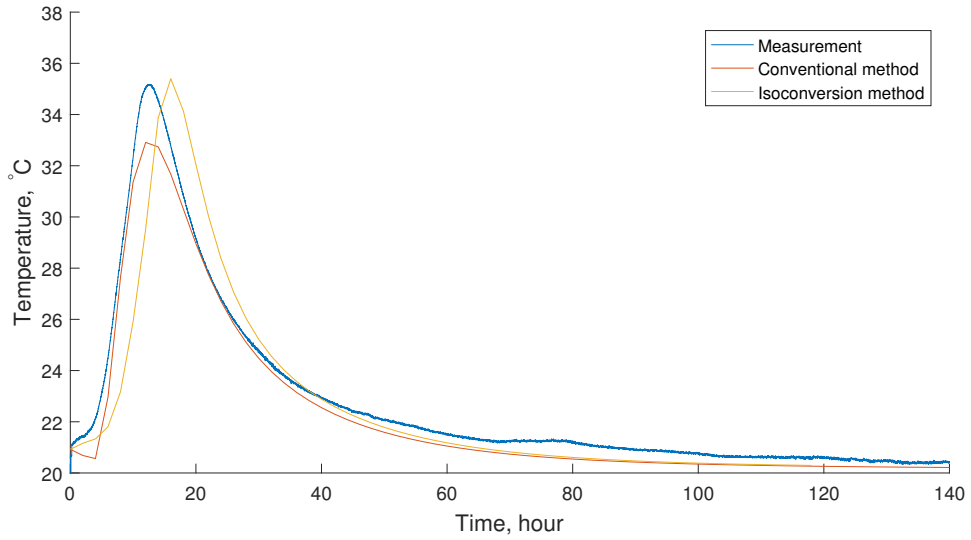

Figure 5.14: Temperature at position of thermocouple 12 from measurements and calculations with conventional- and isoconversional method

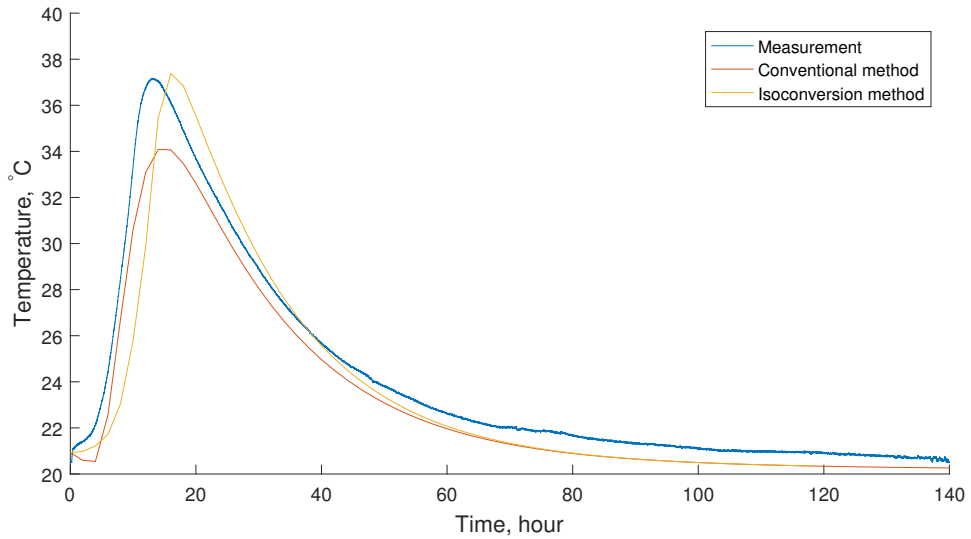

Figure 5.15: Temperature at position of thermocouple 19 from measurements and calculations with conventional- and isoconversional method

In the position of thermocouple 22 the results are similar to the results for thermocouple 1. With the isoconversional method the temperatures are overestimated and the maximum temperature is delayed, whereas for the conventional method the temperature and the time when the max temperature occurs is well estimated.

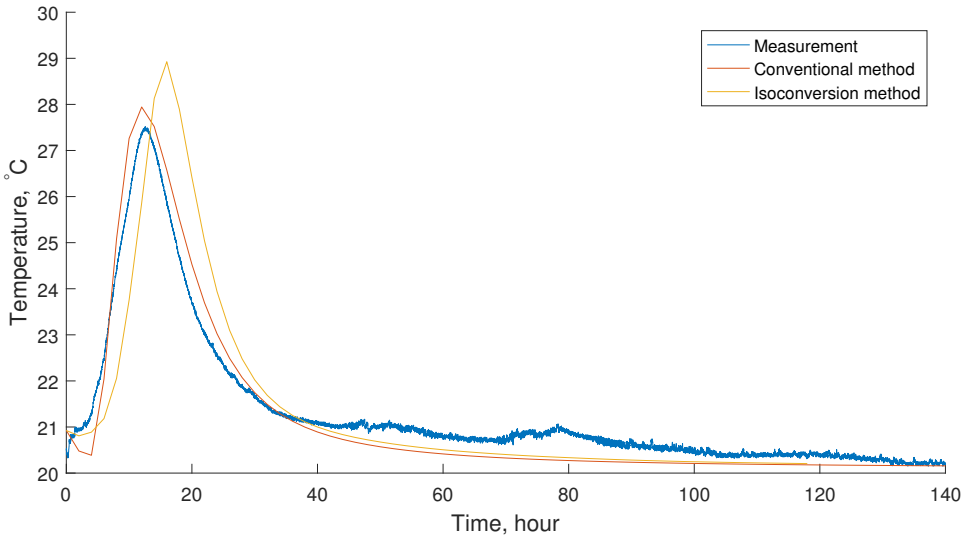

Figure 5.16: Temperature at position of thermocouple 22 from measurements and calculations with conventional- and isoconversional method

With use of the conventional method for the calculations, the peak occurs within 1 hour of the measured one, whereas with use of isoconversional method, the peak consistently lags within 3 hours of the measured one. It was also noted that the simulations with isoconversional method led to much lower temperatures at 10 hours than the temperatures measured and the temperatures computed with the conventional method.

This response of the temperature development was confirmed by comparing the heat development for the different methods, see Appendix A. It was observed that the heat develops slower than for the conventional method but reaches higher heat at later period. Further a simulation was carried out for a material point with adiabatic conditions. Similar to the setup, the isoconversional method had slower temperature rise in early periods but reached higher temperature in later periods, see Appendix B.

5.4.4 Susceptibility of wind velocity

The limitation that 3D modelling is not supported in HACON and assumptions about an axisymmetric geometry had to be made. But it may have been that the asymmetry of the wind velocity due to the fan had a significant influence of the results. Therefore, a study of the wind was made in order to investigate if, and how, the wind influenced the result. This was carried out with a simulation of the

geometry in Figure. 5.17, which is a model of a cross-section of the middle-part of the setup where the insulation is not present.

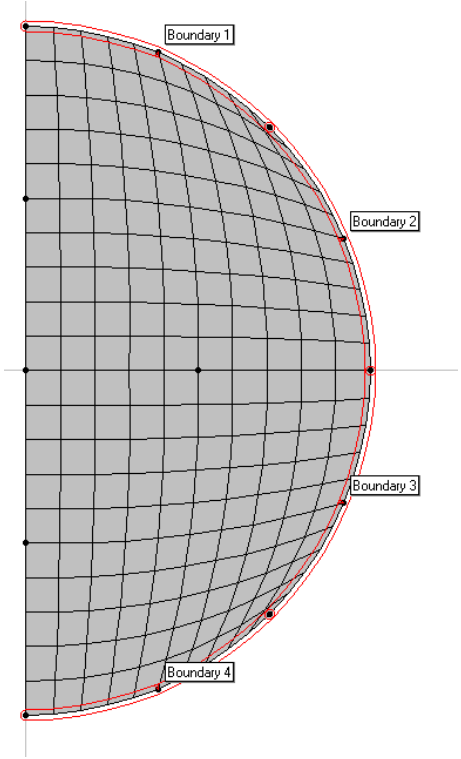

Figure 5.17: Geometry and boundary conditions of the asymmetric wind model with boundary condition 1-4 applied

The simulation was performed to take into account that the wind velocity varies along the boundary, instead of an axisymmetric wind. Just in front of the fan, seen in Figure. 5.4, the wind velocity was assumed to be the highest and decreasing around the boundary. The model consisted of 4 boundaries along the cylinder, each set to individual wind velocities according to Table 5.4. The wind velocities were assumed values, but what is mainly studied is how the temperature develops within the setup with a conceivable more realistic air flow. The material of the model was set to the same concrete in according to Table 5.3 and the simulation is performed with the conventional method.

Table 5.4: Specification of boundary conditions

	"Boundary" 1	"Boundary 2"	"Boundary 3"	"Boundary 4"
Material	PVC	PVC	PVC	PVC
Thickness, mm	3.5	3.5	3.5	3.5
Thermal cond., W/mK	0.16	0.16	0.16	0.16
Wind velocity, m/s	6.0	4.0	2.0	0.0
Avg. temperature, °C	20.92	20.92	20.92	20.92

The results from the simulation are presented in Figure. 5.18, where it can be observed that the hottest part of the pipe is displaced towards the back of the cylinder and therefore, contradicts an axisymmetric model of the setup.

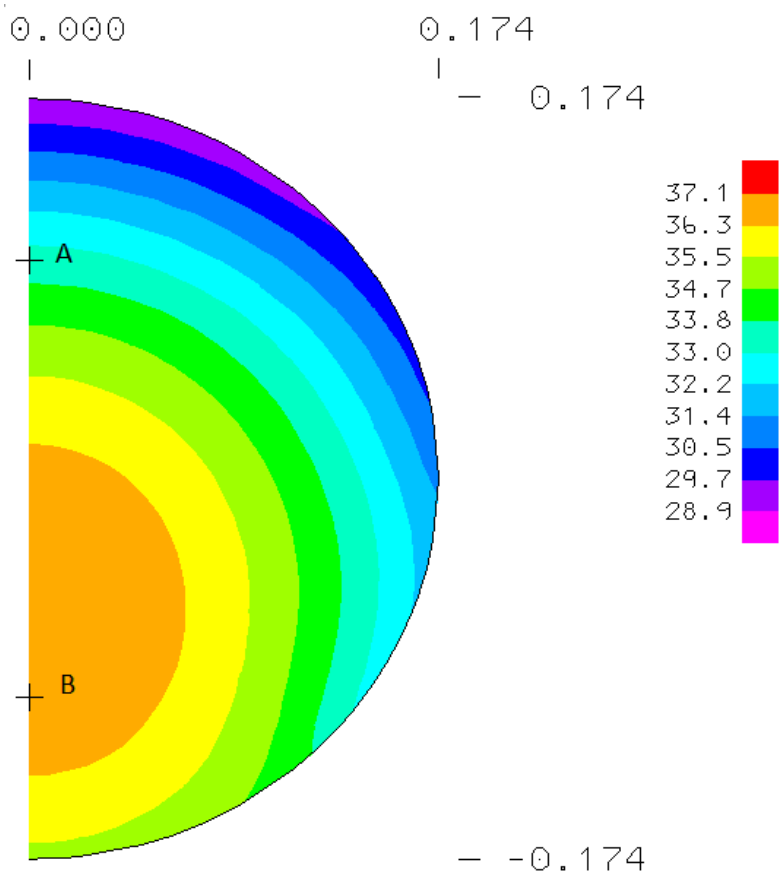

Figure 5.18: Temperature distribution for asymmetric wind model. Point A positioned at (0,0.1) and Point B positioned at (0,-0.1).

The pipe had a diameter of 0.35 m and it isn't trivial whether the temperature development in the asymmetric model can be neglected. Temperatures in two points in the model were extracted to observe how the temperature differed within the setup. In Figure 5.19 the temperature development has been extracted for the point A and B in Figure. 5.18. The observation that can be seen is that although the diameter of the cylinder is fairly small, the temperature difference is approximately 3 °C, see Figure. 5.19.

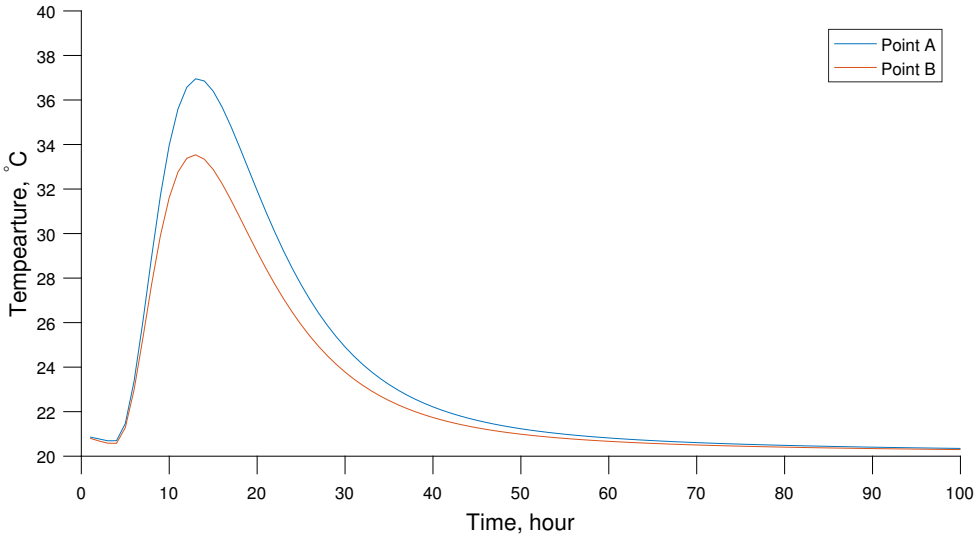

Figure 5.19: Extracted temperature development for point A and B in Figure. 5.18

The primary motive for the fan was just to preserve the prescribed temperature in the boundary condition from the simulation-model. However as, noticed it also affected the temperature distribution and it was observed that the setup was sensitive to the surrounding air flow. As the thickness of the pipe is low and has relatively high thermal conductance, it resulted in high transfer coefficient in combination of the wind velocity. In Figure 5.20, the transfer coefficient from HACON in the boundaries "Edge Low" and "Edge High" for increasing wind velocity is illustrated. It can be noted that transfer coefficient is sensitive for the PVC as it changes considerably in comparison to the EPS for increased wind velocity.

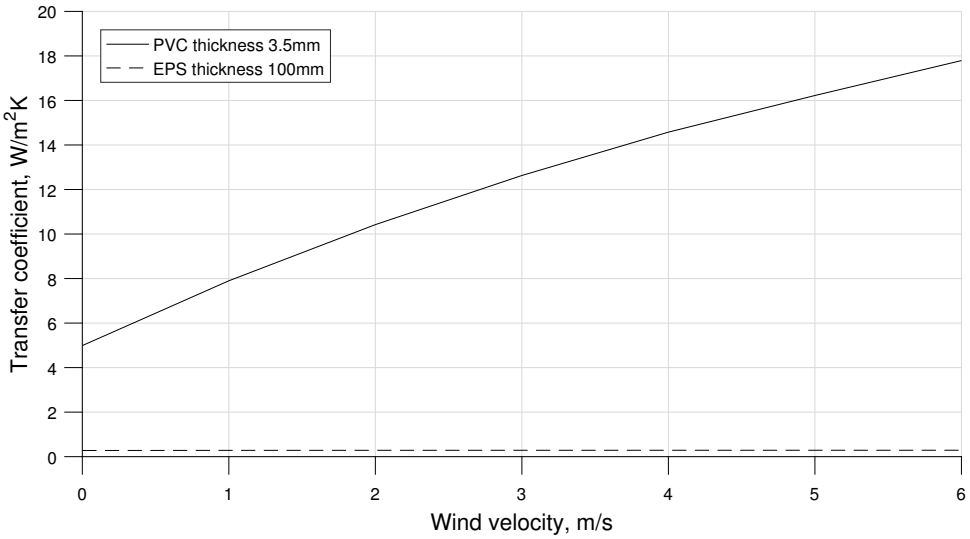

Figure 5.20: Sensitivity of transfer coefficient of boundary "Edge Low" (EPS) and "Edge High" (PVC)

5.4.5 Source of error of the simulation

Material parameters were provided specifically for the concrete in the setup since standard values often apply for concrete where the hydration has progressed for a long period. For earlier periods they don't apply, thus, measurements for the heat capacity, thermal conductivity and density were carried out to provide reliable data.

The wind velocity was not attained quantitatively, so the procedure was to estimate it by adjusting the wind velocity in the model so that temperatures converged with the measurements within a range of -3°C to +3°C. As the temperatures converged with the measurements in most of the positions in the setup, the results were fairly good. With the same conditions applied for the simulation with isoconversional method, the maximum temperatures in the bottom of the setup did not converge as good as the conventional method.

However, it doesn't mean the conventional method to be more accurate as further work needs to be made due to the limitation of 2D and axisymmetric modelling. In general the aerodynamic aspect is not trivial and the observation was that it had a significant influence of the results. Therefore, the question whether the conventional method or the isoconversional method for thermal analysis is more accurate still remains unanswered.

The fan was installed mainly to maintain the temperature of the boundary conditions in the simulation-model by increasing the air flow. However, it was observed when an attempt of a more realistic model of the wind was performed, by varying the wind velocity along the edge, the heat distribution and the temperatures in the model changed considerably. Mainly, it was a consequence of the effect of low thickness

and relatively high thermal conductance of the PVC, which led to a high transfer coefficient in combination of the wind velocity.

The simulation showed temperature differences of approximately 3°C. If the thermocouples were placed on the backside instead, one possibility is that the isoconversional method may have resulted with better confluence, as it was observed in Section 5.4.4 that the temperature were higher on the backside. For future experiments, the uncertainties of the wind can be reduced if the setup is made with consistent surrounding air flow.

6 Concluding Remarks

6.1 Conclusions

The main objective of this dissertation was to develop a routine for computation of thermal power using isothermal calorimetric data, to be used in a finite element simulation program. With this method, the expectations were that this could lead to an improved foundation for thermal analysis of hardening concrete.

The algorithm was developed in Microsoft Visual Studio in the program language Fortran 95 and was successfully implemented for HACON, which is now one of the first programs to support this type of calorimetry. The results from the simulation with the conventional method were then compared to the results from the simulation with the isoconversional method.

It wasn't possible to draw any conclusion of which method is more accurate because of the complex air flow in the setup. Due to the limitation of HACON, the asymmetry of the wind velocity couldn't be taken into account adequately in the simulation. However, the simulations based on the isoconversional method calculated higher temperatures than the simulations using the conventional method.

The experience from this project is that although most factors are deliberately thought out for a setup, there might still be one factor that influence the results considerably. Therefore, further work is needed to verify whether the isoconversional method is more accurate than the conventional.

6.2 Future work

As the heat flow is directly measured with isothermal calorimetry, the heat curves are more accurately attained than with semi-adiabatic calorimetry. The potential to confirm that isoconversional method with finite element analysis is more accurate still exists for future research.

This could be accomplished by isothermal measurements with the same calorimeter for each isothermal run. By performing each isothermal run with the same calorimeter, any deviation between heat conduction calorimeters are accounted equally.

A validation with well-defined boundary conditions should also be made. Mainly consistent air flow surrounding the setup is required, which may be accommodated with a sophisticate setup. By this procedure, an axisymmetric simulation model can be accurately representative of the experimental setup and analysis can be made on reliable basis.

References

[1] Minni Flemark. *Temperaturberäkningar i härdande betongkonstruktioner med indata från isoterm kalorimetri*. Rapport TVBM-5110, Byggnadsmaterial, Lund University, Lund, Sweden. 2017.

[2] Philip Byberger. *En ny metod att hantera temperaturutveckling i härdande betongkonstruktioner - Isoterm kalorimetri används för att mäta värmeutvecklingen i små prover*. Rapport TVBM-5097, Byggnadsmaterial, Lund University, Lund, Sweden. 2014.

[3] O Dahlblom and J Lindemann. *HACON A program for simulation of temperature and stress in hardening concrete*. Report TVSM-3057, Structural Mechanics, Lund University, Lund, Sweden, 2000.

[4] Pierre-Claude Aıtcin and Robert J Flatt. "Portland cement". In: *Science and Technology of Concrete Admixtures*. Woodhead Publishing, 2015. Chap. 3, pp. 27–51.

[5] Dale P Bentz and Pierre-Claude Aitcin. "The hidden meaning of water-to-cement ratio". In: *Concrete international* 30.5 (2008), pp. 51–54.

[6] Hamlin M Jennings, Jeffrey W Bullard, Jeffrey J Thomas, Jose E Andrade, Jeffrey J Chen, and George W Scherer. "Characterization and modeling of pores and surfaces in cement paste". In: *Journal of Advanced Concrete Technology* 6.1 (2008), pp. 5–29.

[7] Jeffrey W Bullard, Hamlin M Jennings, Richard A Livingston, Andre Nonat, George W Scherer, Jeffrey S Schweitzer, Karen L Scrivener, and Jeffrey J Thomas. "Mechanisms of cement hydration". In: *Cement and Concrete Research* 41.12 (2011), pp. 1208–1223.

[8] Pierre-Claude Aıtcin and Robert J Flatt. "Mechanism of cement hydration". In: *Science and Technology of Concrete Admixtures*. Woodhead Publishing, 2015. Chap. 8, pp. 129–145.

[9] Pierre-Claude Aıtcin. "The importance of the water-cement and water-binder ratios". In: *Science and Technology of Concrete Admixtures*. Woodhead Publishing, 2015. Chap. 1, pp. 3–13.

[10] ACI Committee 231. *Early-Age Cracking: Causes, Measurement and Mitigation (231R-10)*. American Concrete Institute, 2010.

[11] Jiong Hu, Zhi Ge, and Kejin Wang. “Influence of cement fineness and water-to-cement ratio on mortar early-age heat of hydration and set times”. In: *Construction and Building Materials* 50 (2014), pp. 657–663.

[12] Dale P Bentz. “Influence of water-to-cement ratio on hydration kinetics: simple models based on spatial considerations”. In: *Cement and Concrete Research* 36.2 (2006), pp. 238–244.

[13] Gyu Don Moon, Sungwoo Oh, Sang Hwa Jung, and Young Cheol Choi. “Effects of the fineness of limestone powder and cement on the hydration and strength development of PLC concrete”. In: *Construction and Building Materials* 135 (2017), pp. 129–136.

[14] Jan Byfors. *Plain concrete at early ages*. Cement-och betonginst., 1980.

[15] JGM De Jong, HN Stein, and JM Stevels. “Hydration of tricalcium silicate”. In: *Journal of Chemical Technology and Biotechnology* 17.9 (1967), pp. 246–250.

[16] HM Jennings and PL Pratt. “An experimental argument for the existence of a protective membrane surrounding Portland cement during the induction period”. In: *Cement and Concrete Research* 9.4 (1979), pp. 501–506.

[17] Paul Barnes and John Bensted. “Hydration of Portland cement”. In: *Structure and Performance of Cements*. 2nd ed. CRC Press, 2002. Chap. 3, pp. 57–113.

[18] HN Stein and JM Stevels. “Influence of silica on the hydration of 3 CaO, SiO2”. In: *Journal of Applied Chemistry* 14.8 (1964), pp. 338–346.

[19] HM Jennings, BJ Dalgleish, and PrL Pratt. “Morphological development of hydrating tricalcium silicate as examined by electron microscopy techniques”. In: *Journal of the American Ceramic Society* 64.10 (1981), pp. 567–572.

[20] Jeffrey J Thomas, Hamlin M Jennings, and Jeffrey J Chen. “Influence of nucleation seeding on the hydration mechanisms of tricalcium silicate and cement”. In: *The Journal of Physical Chemistry C* 113.11 (2009), pp. 4327–4334.

[21] Sandrine Garrault and André Nonat. “Hydrated layer formation on tricalcium and dicalcium silicate surfaces: experimental study and numerical simulations”. In: *Langmuir* 17.26 (2001), pp. 8131–8138.

[22] AGA Saul. “Principles underlying the steam curing of concrete at atmospheric pressure”. In: *Magazine of Concrete Research* 2.6 (1951), pp. 127–140.

[23] P Freiesleben Hansen and Erik J Pedersen. *Maturity computer for controlled curing and hardening of concrete*. Tech. rep. 1977.

[24] Nicholas J Carino. “The maturity method: theory and application”. In: *Cement, concrete and aggregates* 6.2 (1984), pp. 61–73.

[25] AB Svensk Byggtjänst, Börtemark Ingvar, Möller Göran, and Petersons Nils. “Betong handboken”. In: *Material, AB Svensk Byggtjänst och Cementa AB, Stockholm* (1997).

[26] Jan-Erik Jonasson. “Modelling of temperature, moisture and stresses in young concrete”. PhD thesis. Luleå tekniska universitet, 1994.

[27] SBUF. *Produktionsplanering Betong*. URL: http://www.sbuf.se/Nyheter-och-publikationer/Aktuellt/2014/PPB/.

[28] Rupert Springenschmid. *Prevention of thermal cracking in concrete at early ages*. Vol. 15. CRC Press, 1998.

[29] L Wadsö. "An experimental comparison between isothermal calorimetry, semi-adiabatic calorimetry and solution calorimetry for the study of cement hydration". In: *Nordtest report TR* 522 (2003).

[30] Peter Fjellström, Jan-Erik Jonasson, Mats Emborg, and Hans Hedlund. "Heat loss compensation for semi-adiabatic calorimetric tests". In: *Nordic Concrete Research* 47.1 (2013), pp. 39–60.

[31] Wilson Ricardo Leal da Silva, Vıt Šmilauer, and Petr Štemberk. "Upscaling semi-adiabatic measurements for simulating temperature evolution of mass concrete structures". In: *Materials and Structures* 48.4 (2015), pp. 1031–1041.

[32] Peter Šimon. "Isoconversional methods". In: *Journal of Thermal Analysis and Calorimetry* 76.1 (2004), p. 123.

[33] Lars Wadsö. "Operational issues in isothermal calorimetry". In: *Cement and Concrete Research* 40.7 (2010), pp. 1129–1137.

[34] Sergey Vyazovkin, Alan K Burnham, José M Criado, Luis A Pérez-Maqueda, Crisan Popescu, and Nicolas Sbirrazzuoli. "ICTAC Kinetics Committee recommendations for performing kinetic computations on thermal analysis data". In: *Thermochimica Acta* 520.1 (2011), pp. 1–19.

[35] Niels Saabye Ottosen and Hans Petersson. *Introduction to the finite element method*. Prentice-Hall, 1992.

[36] Jan-Erik Jonasson and Peter Fjellström. *Mätning och modellering av hållfasthets- och värmeutveckling för betonger med Svenska Cement*. 2011.

Appendices

A Produced heat at 20°C

Due to different procedures when establishing the heat produced for semi-adiabatic measurements and isothermal measurements, it is of interest to compare how the heat diverges from each other when they are established for the same cement. The heat curve was established for the isothermal calorimetry with measurements and the heat curves for the conventional method was calculated according to Eq. (2.10) with use of data for the cement, see Table 5.3.

Figure 1 illustrates the produced heat over time for an isotherm of 20°C and it can be noted that the heat developments are slightly different. The conventional method, where a set of fitting parameters has been established, results in higher heat rate in early periods until a certain time, where the heat rate decreases. Unlike the conventional method, the isothermal calorimetry results in a slower heat rate in early periods but gradually passes the conventional method with higher heat produced. From the heat curves seen in Figure. 1, it seems expected that at the same time t in early periods, simulations with isothermal measurements produce lower heat than the conventional method. The same behaviour was noticeable from simulations, shown in Section 5.4.1.

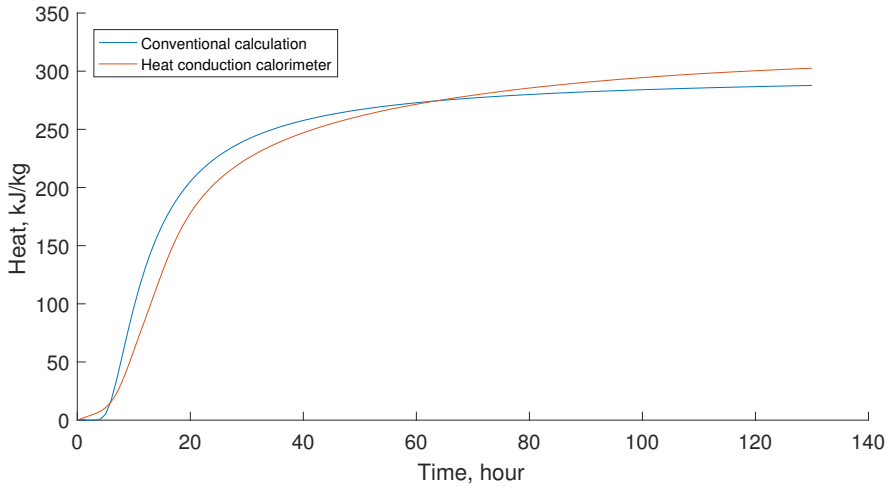

Figure 1: Heat developments with the heat conduction calorimeter and with the conventional calculation

B Adiabatic temperature rise of material point

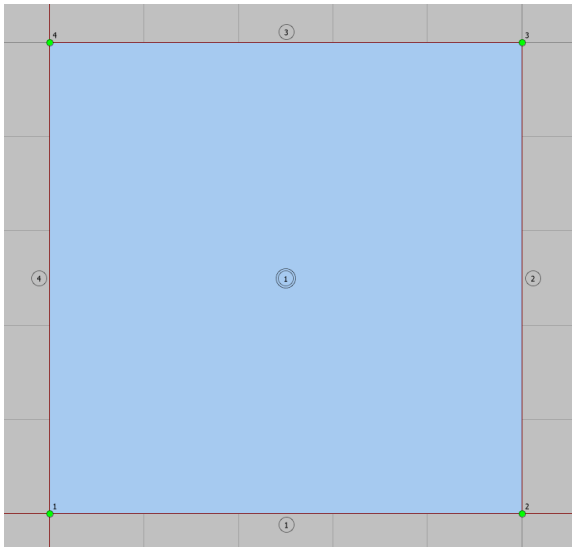

Figure 2: Verification model consisting of 1 element

In order to observe the characteristics of the conventional and isoconversional method, an adiabatic simulation of the model in Figure. 2 was performed, which was based on one element. It's seen that the isoconversional method has lower temperature in early periods (6h-13h) but reaches higher temperatures at later periods.

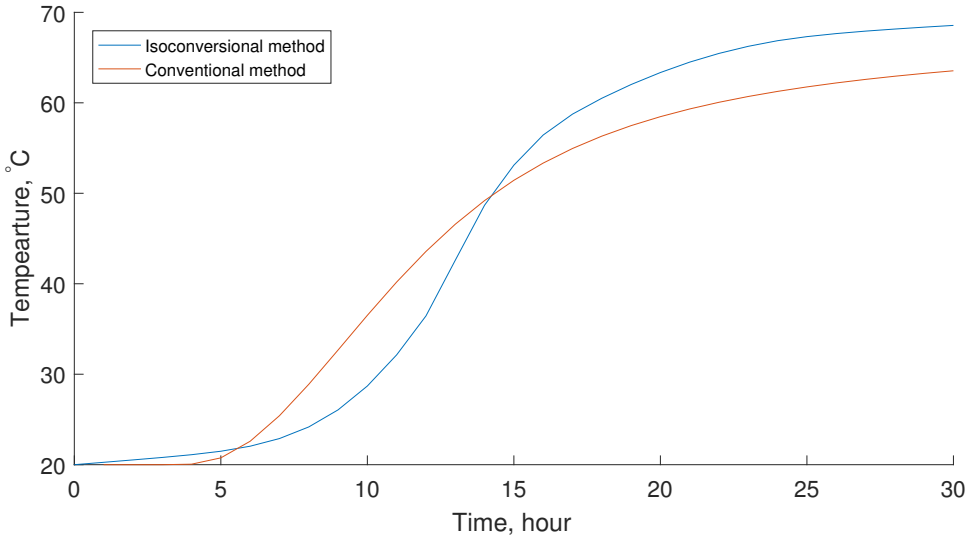

Figure 3: Calculated adiabatic temperature rise with conventional and isoconversional method for a material point

C Errors of linear approximation

In each material point where a temperature development is proceeding, an interpolation is made in the curve set to extract corresponding thermal power for each temperature and degree of hydration. However, one must be careful when interpreting the results as the interpolation may involve errors of the extracted thermal power. In following figures the linear relation between each isotherm will be presented for various degrees of hydration. It can be observed that the goodness of the regression between the isotherms depends on the degree of hydration where a low degree of hydration, results in good estimation of the thermal output, where as the higher the degree of hydration progresses the error of the estimated thermal power increases.

Degree of hydration 0.0 to 0.3

Regression in the logarithmic domain of the isotherms in the interval of 0.0 and 0.3 degree of hydration presented in Figure 5.

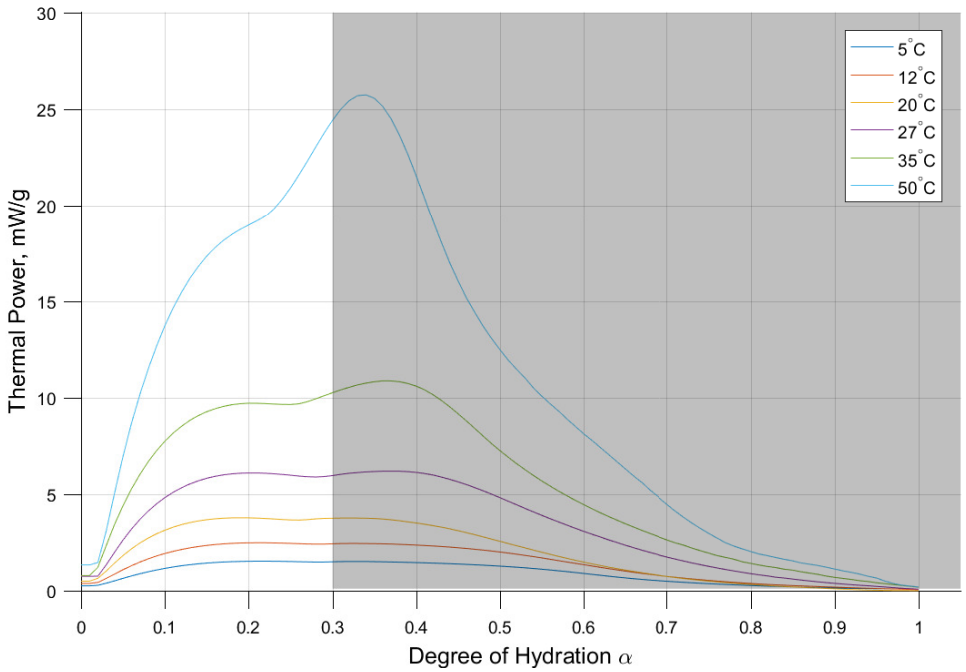

Figure 4: Study of $\alpha = 0.0$ to $\alpha = 0.3$

For $\alpha = 0.0$ the error is larger than for $\alpha = 0.1$ to $\alpha = 0.3$. However, it's possible that this is due to noise that often happens when the measurements begin. For values of α higher than 0.0, it's noticeable that the error of the regression is fairly small for $\alpha = 0.1$ to $\alpha = 0.3$. This implies that the interpolation in the interval of $\alpha = 0.1$ to $\alpha = 0.3$ is reliable, independent of the temperature between 5°C and 50°C.

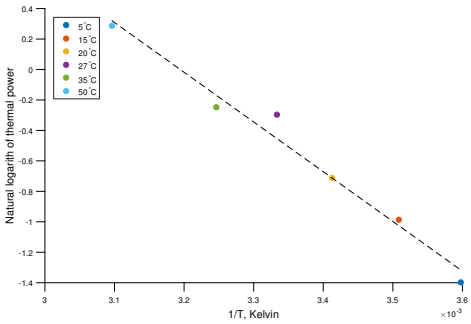

(a) Linear regression for $\alpha = 0.0$

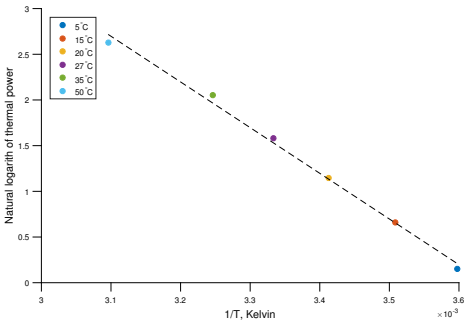

(b) Linear regression for $\alpha = 0.1$

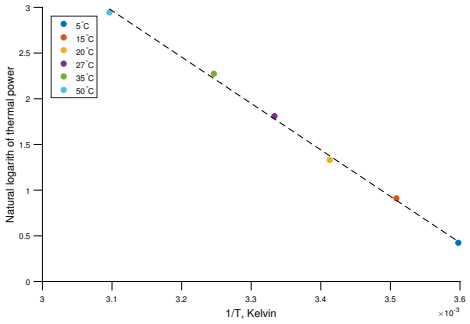

(c) Linear regression for $\alpha = 0.2$

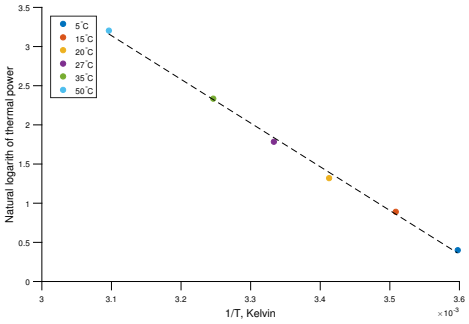

(d) Linear regression for $\alpha = 0.3$

Figure 5: Linear relation of $\alpha = 0.0$ to $\alpha = 0.3$ in the logarithmic domain. Y-axis is ln(thermal power) and x-axis is $1/T$, where T is in Kelvin.

Degree of hydration 0.35 to 0.6

Regression in the logarithmic domain of the isotherms in the interval of 0.3 and 0.6 degree of hydration presented in Figure 7.

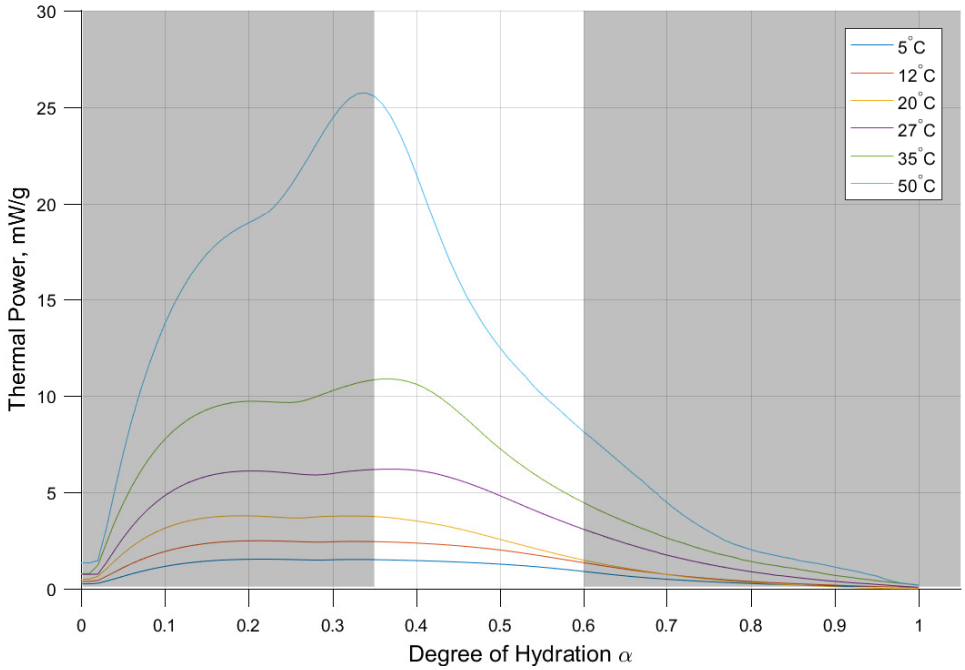

Figure 6: Study of $\alpha = 0.35$ to $\alpha = 0.6$

In Figure 7 it can be noted that the error becomes slightly larger, but it is still reasonably low. The same cannot be said for $\alpha = 0.55$ and $\alpha = 0.65$ where the error for 20°C has become larger than the other temperatures. It's unexpected that the 20°C data deviates that much from the others and it could be explained either as an outliar or it may have been an error of the measurement for that temperature.

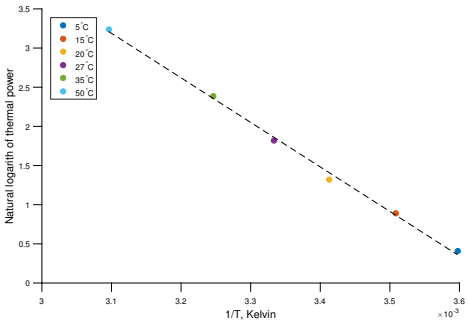

(a) Linear regression for $\alpha = 0.35$

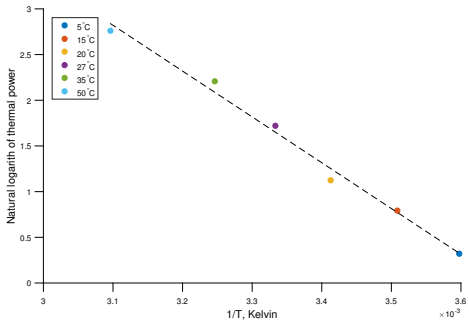

(b) Linear regression for $\alpha = 0.45$

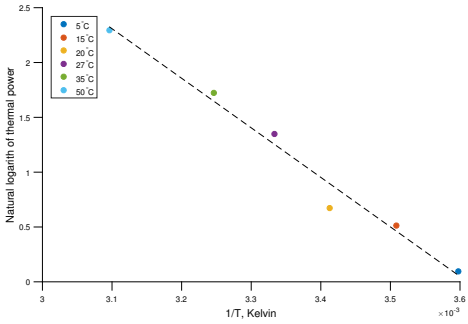

(c) Linear regression for $\alpha = 0.55$

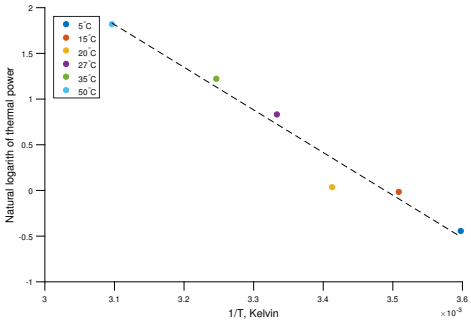

(d) Linear regression for $\alpha = 0.6$

Figure 7: Linear relation of $\alpha = 0.35$ to $\alpha = 0.6$ in the logarithmic domain. Y-axis is ln(thermal power) and x-axis is $1/T$, where T is in Kelvin.

Degree of hydration 0.7 to 1.0

Regression in the logarithmic domain of the isotherms in the interval of 0.6 and 1.0 degree of hydration presented in Figure 9.

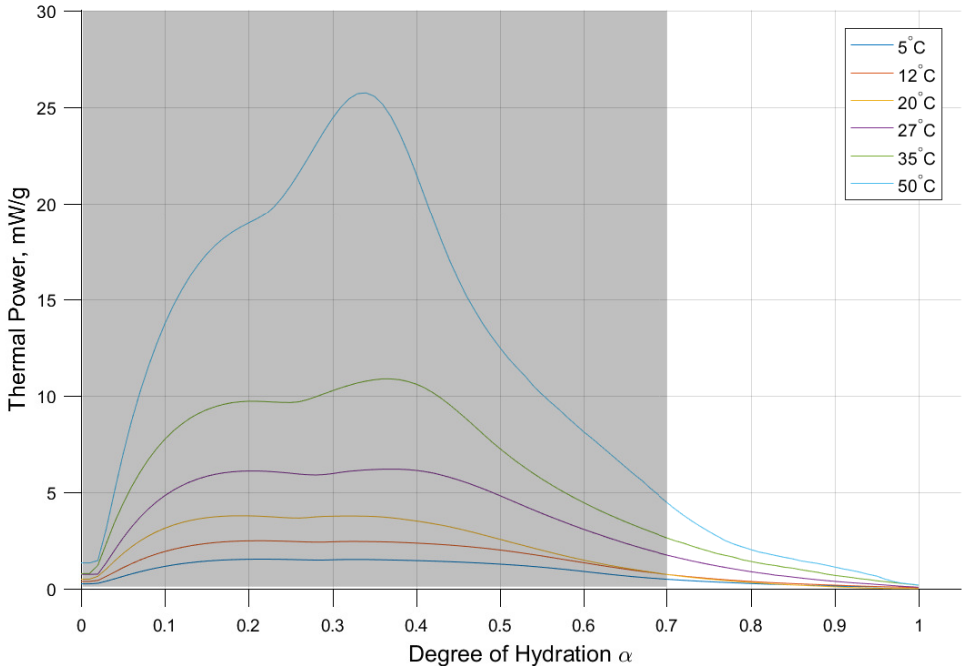

Figure 8: Study of $\alpha = 0.7$ to $\alpha = 1.0$

It can be noted that the error increases as the degree of hydration increases. One hypothetical factor that could explain the response is that the chemical reaction in the concrete reduces. In earlier periods, the produced heat is mainly due to chemical reactions, however, for higher degree of hydration the cement is more prone to other reactions than chemical. For example when the structure becomes more compact the cement particles are not surrounded by water and in order for the cement and water to react, will be through diffusion. The Arrhenius equation is a function that describes chemical reactions and that may be the reason that there's a good fit in earlier periods, but not in later periods. Hence, the error increases and the Arrhenius equation may not be adequate to fully describe the temperature dependence for high values of α. For high values of α the results should be taken cautiously since that is the part where the extrapolation are made.

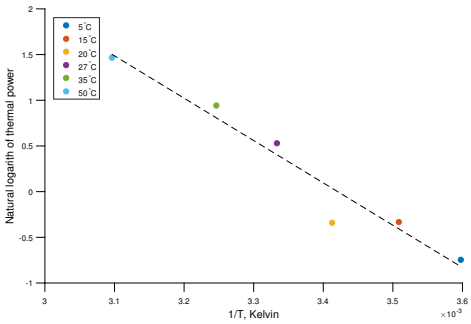

(a) Linear regression for $\alpha = 0.7$

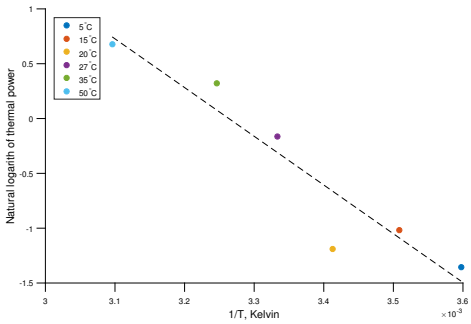

(b) Linear regression for $\alpha = 0.8$

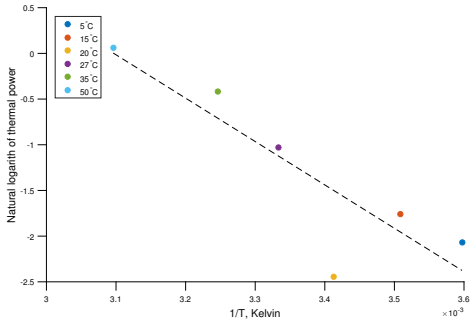

(c) Linear regression for $\alpha = 0.9$

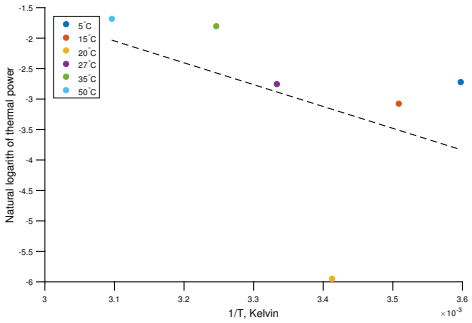

(d) Linear regression for $\alpha = 1.0$

Figure 9: Linear relation of $\alpha = 0.7$ to $\alpha = 1.0$ in the logarithmic domain. Y-axis is ln(thermal power) and x-axis is $1/T$, where T is in Kelvin.

D Simulation with linear least square and linear interpolation

The linear least square method is mostly used if the data is expected to be noisy. However, one idea was to interpret the deviation from the regression line as the true temperature dependence, not interpreting the deviation as noise. One reason for this implementation was to examine if it could have any significant influence of the results from the simulation. Hence, a second algorithm was also developed but with use of simple linear interpolation which only interpolated between the 2 closest temperatures for the temperature of interest.

A simulation of the model in Figure. 2 was performed for the new algorithm. The temperature rise obtained with different interpolation methods can be observed in Figure. 10, where the differences in temperature are minimal.

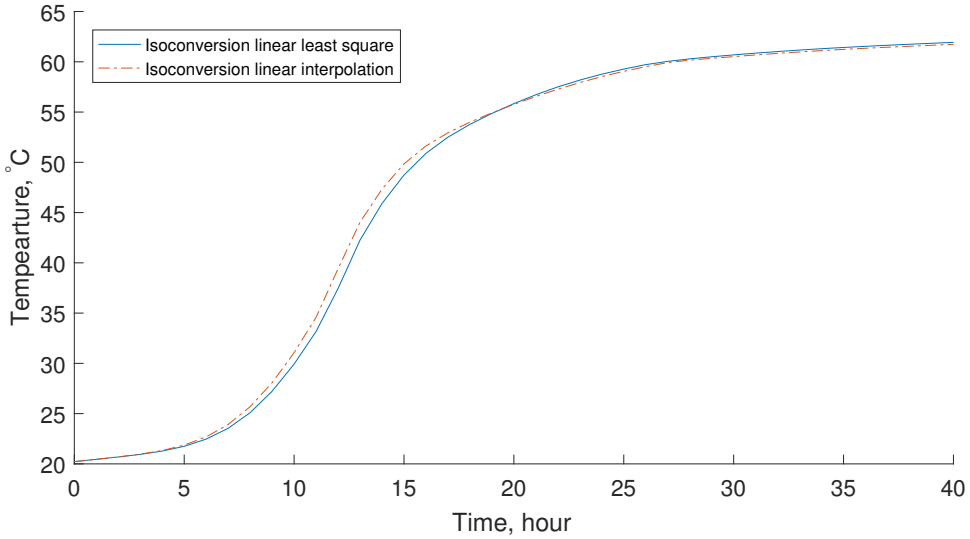

Figure 10: Calculated adiabatic temperature using linear least square and linear interpolation